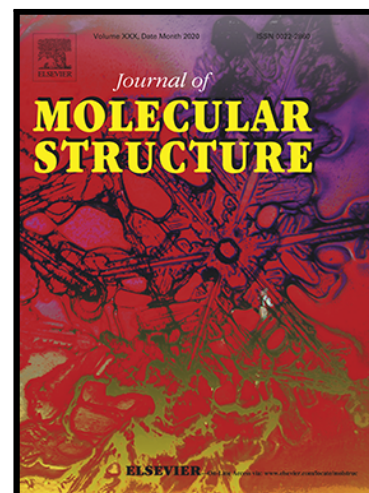


Journal Pre-proof

Synthesis, crystal structure, Hirshfeld surface analysis, spectral characterization, reduced density gradient and nonlinear optical investigation on (E)-N'-(4-nitrobenzylidene)-2-(quinolin-8-yloxy) acetohydrazide monohydrate: A combined experimental and DFT approach



Oumeria Kourat , Ahmed Djafri , Nadia Benhalima ,
Youcef Megrouss , Nour El Houda Belkafouf , Rachida Rahmani ,
Jean-Claude Daran , Ayada Djafri , Abdelkader Chouaih

PII: S0022-2860(20)31272-2
DOI: <https://doi.org/10.1016/j.molstruc.2020.128952>
Reference: MOLSTR 128952

To appear in: *Journal of Molecular Structure*

Received date: 1 June 2020
Revised date: 18 July 2020
Accepted date: 20 July 2020

Please cite this article as: Oumeria Kourat , Ahmed Djafri , Nadia Benhalima , Youcef Megrouss , Nour El Houda Belkafouf , Rachida Rahmani , Jean-Claude Daran , Ayada Djafri , Abdelkader Chouaih , Synthesis, crystal structure, Hirshfeld surface analysis, spectral characterization, reduced density gradient and nonlinear optical investigation on (E)-N'-(4-nitrobenzylidene)-2-(quinolin-8-yloxy) acetohydrazide monohydrate: A combined experimental and DFT approach, *Journal of Molecular Structure* (2020), doi: <https://doi.org/10.1016/j.molstruc.2020.128952>

This is a PDF file of an article that has undergone enhancements after acceptance, such as the addition of a cover page and metadata, and formatting for readability, but it is not yet the definitive version of record. This version will undergo additional copyediting, typesetting and review before it is published in its final form, but we are providing this version to give early visibility of the article. Please note that, during the production process, errors may be discovered which could affect the content, and all legal disclaimers that apply to the journal pertain.

© 2020 Published by Elsevier B.V.

Highlights

- A novel quinoline derivative was synthesized and characterized.
- FT-IR, NMR, UV–Vis techniques and DFT method were used to investigate.
- Conformational analysis was performed to determine the stable geometry.
- Theoretical spectroscopic properties of NBQA were examined by BPV86 functional.
- The complete vibrational assignment and spectroscopic analysis have been carried out.
- The HS, NBO and RDG analyses explained the intramolecular hydrogen bonding.
- First hyper polarizability and HOMO-LUMO energy gap were theoretically predicted.

Journal Pre-proof

Synthesis, crystal structure, Hirshfeld surface analysis, spectral characterization, reduced density gradient and nonlinear optical investigation on (E)-N'-(4-nitrobenzylidene)-2-(quinolin-8-yloxy) acetohydrazide monohydrate: A combined experimental and DFT approach

Oumeria Kourat,^{a,b} Ahmed Djafri,^{a,c} Nadia Benhalima,^{a,d} Youcef Megrouss,^a Nour El Houda Belkafouf,^a Rachida Rahmani,^{a,e} Jean-Claude Daran,^f Ayada Djafri^g and Abdelkader Chouaih^{a,*}

Dedicated to the memory of our friend and colleague Prof. Dr. Fodil Hamzaoui

^a Laboratory of Technology and Solid Properties (LTPS), Abdelhamid Ibn Badis University of Mostaganem, 27000 Mostaganem, Algeria

^b Chemistry department, Faculty of Sciences and Technology, Dr. Tahar Moulay University of Saida - POBox 138, 20002 Saida, Algeria

^c Centre de Recherche Scientifique et Technique en Analyses Physico-chimiques (CRAPC), BP 384, Bou-Ismaïl-RP, 42004, Tipaza, Algeria

^d Physics Department, Faculty of Sciences, Dr. Tahar Moulay University of Saida - POBox 138, 20002 Saida, Algeria

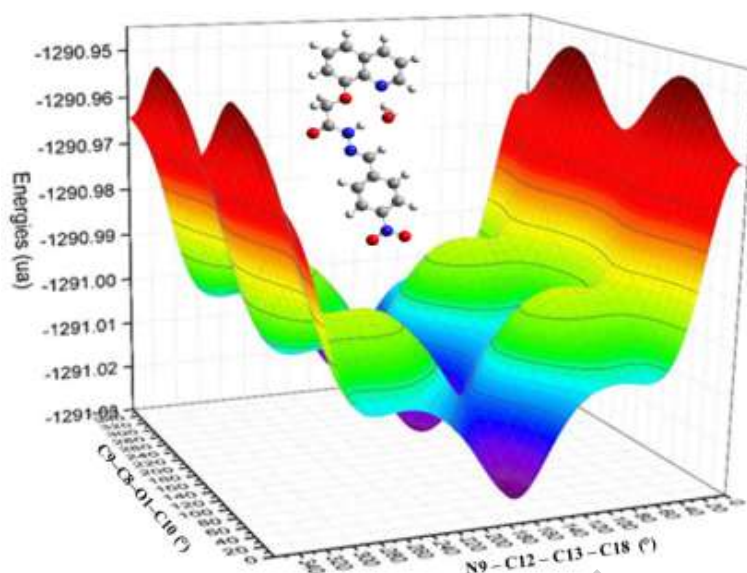
^e Département de Génie des Procédés, Centre Universitaire Ahmed Zabana - Relizane, 48000 Relizane, Algeria

^f Laboratoire de Chimie de Coordination, UPR-CNRS 8241, 205, route de Narbonne, 31077 Toulouse Cedex, France

^g Laboratory of Organic Applied Synthesis (LSOA), Department of Chemistry, Faculty of Sciences, University of Oran 1, Ahmed Ben Bella, 31000 Oran, Algeria

*Correspondence e-mail: achouaih@gmail.com, abdelkader.chouaih@univ-mosta.dz

Graphical abstract



Abstract

In this work, (E)-N'-(4-nitrobenzylidene)-2-(quinolin-8-yloxy) acetohydrazide monohydrate (NBQA) crystal was synthesized and its structural characterization was carried out by single-crystal X-ray diffraction. The intermolecular interactions in the crystal were investigated through the Hirshfeld surface analysis and the 2D-fingerprint plot. In the solid phase, the spectroscopic characterization was also carried out using FT-IR, ^1H -NMR, and ^{13}C -NMR experimental spectroscopies. To support experimental results, DFT calculations have been accomplished on the NBQA molecule in the ground state. First, theoretical calculations were performed using BPV86 and GGA-PBE functionals with the 6-311G(d,p) basis set to obtain the stable conformer of the molecule. Likewise, harmonic vibrational frequencies, ^1H and ^{13}C chemical shifts, and NBO analysis were also calculated using the same level of theory and compared to available experimental data. Furthermore, the molecular electrostatic potential (MEP), frontier molecular orbitals (FMO) analysis, HOMO-LUMO energies, energy band gap, density of state (DOS), global chemical reactivity descriptors, and some thermodynamic functions were studied and discussed. UV-Vis spectrum was predicted by the TD-DFT method in chloroform solvent and compared with the experimental spectrum for displaying the involved electronic transitions in the compound. The repulsive, attractive, and Van der Waals strong and weak interactions in NBQA were investigated via the RDG analysis. The NLO properties of NBQA have also investigated in different available solvents by DFT and compared to the most important compounds in the field. The first hyperpolarizability values

of NBQA have been increased with increasing solvent polarity and decreasing the energy band gap.

Keywords: Quinoline, H-bonding, NLO, DOS, NBO, electronic transitions

Journal Pre-proof

1. Introduction

Quinoline derivatives are of interest class of bicyclic nitrogen-containing aromatic compounds. They are attracting a considerable deal of attention owing to their implication in various research works, their wide spectrum of biological properties, and their presence in naturally occurring compounds [1]. As evidence of these properties, they can be found in many drugs such as antibiotics, antimalarial, antidiabetics, anti-inflammatories [2-4]. Besides, polysubstituted quinoline can achieve hierarchical self-assembly into a variety of meso and nanostructures with enhanced photonic and electronic properties [5]. They are also used in the synthesis of molecules having nonlinear optical (NLO) properties [6,7]. On the other hand, quinoline-based hydrazones are known for their excellent biological and biochemical activities. Otherwise, the synthetic flexibility of quinoline hydrazones allows the generation of a broad spectrum of structurally diverse derivatives [8,9]. As it is well known, in organic frameworks with large delocalized π -systems, π -electrons are more polarizable due to their further enhancement by the incorporation of donor and acceptor substituents at the extremities of the conjugated system [10]. These groups at the opposite ends are strongly responsible for the charge transfer magnitude. The NLO activity, measured by the value of first hyperpolarizability (β), results from the movement of electrons in the entire molecule from electron-donor to electron-acceptor groups. Molecules with high hyperpolarizability values can be developed into NLO materials which have potential applications in optoelectronic devices in telecommunications, information storage, optical switching, and photovoltaic devices such as solar cells [11,12]. The research of new NLO materials is largely based on the theoretical prediction of precise electro-optical properties for the above-mentioned systems. The theoretical calculation, and more precisely density functional theory (DFT) approach, is currently the first procedure for studying NLO responses and their relation to structural features [13].

The identification of the molecular structure of organic compounds requires different techniques and approaches. Structural elucidation of unknown small molecules has been always one of the most important applications of molecular spectroscopy. Although, the strategies to confirm the presence of compounds by spectroscopy techniques with structure elucidation are well known. The most important analytical techniques to identify unknown small organic molecules are nuclear magnetic resonance spectroscopy (NMR) or infrared spectroscopy and X-ray crystallography and other spectroscopic methods. Modern structure elucidation using a combination of the above mentioned analytical techniques has enabled

chemists to investigate large and complex biomolecules. Nowadays, experimental techniques are not sufficient to fully characterize a molecular structure. However, these techniques are used in combination with theoretical methods. In addition, computational methods can be an important asset in improving the capabilities and efficiency of the elucidation process. Modern quantum chemical methods with the appropriate level of theory and basis set are used in our study with a view to performing conformational analysis, elucidating the electronic structure, and predicting the corresponding vibrational properties. Computational studies, based on density functional theory, have played an integral role in determining planar structures and stereochemical configurations of the title molecule. Herein, we describe and discuss the elucidation of the structure of a quinoline derivative based on spectroscopic, chemical, and computational tools. On the other hand, the computational approach can be used to calculate properties that were not reported by the experiment.

In a continuation of our recent research on the development of organic heterocyclic compounds [14-19] and given the importance of quinolines, this paper reports the synthesis, molecular structure and the Hirshfeld surface description of a new quinoline derivative, namely (E)-N-(4-Nitrobenzylidene) 2-(8-quinolyloxy) aceto hydrazide monohydrate (NBQA). In the present study, both experimental and molecular modeling are combined for studying the potential energy surface (PES), molecular structural parameters, vibrational spectra, ^1H and ^{13}C nuclear magnetic resonance (NMR) chemical shifts, UV-Vis transitions, HOMO-LUMO energies, charge distribution, reduced density gradient (RDG) isosurface, total dipole moment, polarizability and first-order hyperpolarizability (β), The global reactivity descriptors, namely, hardness, softness, chemical potential, electrophilicity index, and thermodynamical functions are also calculated to understand the reactive nature of the compound. In this work, all theoretical calculations were performed using the DFT method with BPV86 and GGA-PBE functionals. These functionals associated with the DFT method have been previously shown to provide an excellent compromise between experimental and computational efficiency of molecular geometry, vibrational frequencies, atomic charges, global chemical reactivity descriptors, thermodynamical functions, and especially NLO properties for large and medium-size molecule [20-22]. Therefore, the BPV86/6-311G (d, p) and PBE/6-311G (d, p) methods are chosen for the calculation in this work.

2. Experimental and computational details

2.1. Synthesis, crystallization and spectral measurements

The NBQA compound was synthesized as indicated by the chemical pathways in scheme 1. The condensation of 8-hydroxyquinoline (0.01 mol) (1) along with ethyl bromoacetate (0.01 mol) in dry acetone for 12 hours in the presence of anhydrous K_2CO_3 yielded ethyl(quinolin-8-yloxy)acetate (2). The latter (0.01 mol) was mixed with hydrazine hydrate (0.02 mol) in ethanol and the mixture was refluxed for 1 hour. The obtained solid was isolated, washed with cold water, filtered, dried, and recrystallized from ethanol to yield 2-(quinolin-8-yloxy)acetohydrazide (3). Thereafter, para-nitrobenzaldehyde (0.01 mol) was added to a solution of the obtained intermediate (compound 3) (0.01 mol) in absolute ethanol to obtain compound (4). Then, the title compound (E)-N'-(4-nitrobenzylidene)-2-(quinolin-8-yloxy)acetohydrazide (4) with moderate yield 75% and melting point $211^\circ C$ was filtered and dried after refluxing for 12 hours. Single crystals of the title compound suitable for X-ray diffraction were obtained with recrystallization from ethanol solution.

FT-IR spectral characterization was performed on a JASCOFT/IR4200 Fourier transform infrared spectrometer. FT-IR spectrum ($4000-400\text{ cm}^{-1}$) was recorded as KBr pellets in the solid phase at room temperature with the number of scans 8 and resolution 4 cm^{-1} . 1H and ^{13}C -NMR spectra were recorded with a Bruker AC250 spectrometer at $25^\circ C$ in deuteriochloroform solution. Chemical shifts are given as δ (ppm) relative to tetramethylsilane (TMS) as an internal standard. The ultraviolet absorption spectrum of NBQA was measured in deuteriochloroform solution using a Unicam UV2 spectrophotometer in the range of 200–800 nm.

IR (KBr, cm^{-1}): 3466 (N–H, CONH), 1674 (C=N), 1184 (N–N), 1084 (C–O–C), 749 (C–H); 1H NMR ($CDCl_3$, 500 MHz) δ (ppm) : 12.49 (s, 1H, N-H), 8.96 (d, 1H, H-quinolin near N), 8.48 (s, 1H, N=CH), 8.28-7.33 (m, 9H, Ar-H), 4.99 (s, 2H, OCH_2); ^{13}C NMR ($CDCl_3$, 125 MHz) δ (ppm): 176.44(C=O), 165.76, 165.01(C- NO_2), 154.25(C=N quinolin), 152.21, 148.99, 148.67, 146.02, 139.85, 137.09, 129.79, 128.27, 127.29, 123.92, 122.71, 122.14, 114.88, 71.44 (O- CH_2).

Scheme 1

2.2. X-ray data collection and structure determination

A single crystal with dimensions of $0.20 \times 0.15 \times 0.10$ mm was used for the collection of X-ray diffracted intensities. Raw data have been obtained with Bruker APEX II Quazar four-circle diffractometer with graphite monochromated $MoK\alpha$ radiation ($\lambda = 0.71073\text{ \AA}$). Data reduction and integration were performed with the help of SAINT [23]. Peak indexing was

carried out using APEX2 [24]. The SADABS program [25] was used to apply absorption correction. In addition, the programs Shelxs and Shelxl were used to solve and refine the structure [26,27]. The refinement was carried out by using the Full matrix least square on F₂. All non-hydrogen atoms were refined anisotropically by considering all reflections with $I \geq 2\sigma(I)$. The 16 hydrogen atoms of NBQA were fixed geometrically without any constraints and refined with isotropic thermal coefficients. The Olex-2 program [28] was used for visualization of the crystal structure. Experimental, crystallographic, and refinement details for NBQA are summarized in Table 1.

Table 1

2.3. Computational details

All the theoretical calculations for the title compound were carried out with the assistance of Gaussian 09 software package [29] using BPV86 (Burke and Perdew's 1986 functional with correlation replaced by Vosko et al.) [30,31] and GGA-PBE (the 1996 exchange functional of Perdew, Burke, and Ernzerhof) [32] methods in conjunction with 6-311G (d, p) basis set. The molecular structures were visualized employing the GaussView program [33]. The theoretical vibrational spectra of the title compound and their detailed assignments were performed and interpreted based on potential energy distribution (PED) analysis by using the VEDA 4 program [34]. ¹H and ¹³C chemical shifts were calculated with the gauge-independent atomic orbital (GIAO) approach using corresponding TMS shielding calculated at the BPV86/6-311G(d,p) level. The natural bond orbital (NBO) analysis was performed using the NBO 3.1 program [35]. Ultraviolet-visible spectra, excitation energies, absorbance, and oscillator strengths for the title compound at the ground state optimized geometry were obtained in the framework of TD-DFT [36,37] calculations with the BPV86/6-311G(d,p) and GGA-PBE/6-311G(d,p) methods. Moreover, the HOMO and LUMO together with the band-gap energies were calculated using the same level of theory. The density of states (DOS) diagram of the title compound has been obtained and plotted by the GaussSum 2.2 program [38]. Molecular electrostatic potential (MEP) surface was investigated by using BPV86 and GGA-PBE functionals with a 6-311G (d, p) basis set using the Gaussian 09 program. RDG and sgn(λ_2) ρ functions were computed using Multiwfn [39] and drawn with the VMD program [40], respectively. DFT calculations were also used to reach the dipole moment, the mean polarizability, and the total first static hyperpolarizability in different solvents.

3. Results and discussion

3.1. Potential energy surface (PES) scans study

Due to the flexibility of (E)-N'-(4-nitrobenzylidene)-2-(quinolin-8-yloxy) acetohydrazide monohydrate (NBQA) and possible rotational isomerism, the potential energy surface (PES) scans are performed. The conformational study was carried out to obtain the most stable conformers of the title compound by using the BPV86/6-311G(d,p) calculation level of density functional theory. In this context, the dihedral angles C9–C8–O1–C10 and N9–C12–C13–C18 are suitable coordinates for the flexibility of conformation within the molecule. During the scan procedure, the entire geometrical parameters were simultaneously relaxed, while the C9–C8–O1–C10 and N9–C12–C13–C18 dihedral angles were varied in steps of 2° ranging from 0° to 360°. 3D PES highlighting the variation of dihedral angles (C9–C8–O1–C10 and N9–C12–C13–C18) and their relative energies are displayed in Fig. 1. The graph clearly shows that there is one conformer at the minimum energy level. The local minimum is observed at ($\theta_1 = 176^\circ$ and $\theta_2 = 180^\circ$) dihedral angles with an energy value of -1291.0255 Hartree. The obtained geometry was confirmed by the frequency analysis as minima with no imaginary frequency.

Figure 1

3.2. Geometry description

The single-crystal X-ray analysis reveals that the NBQA compound crystallizes in the monoclinic space group $P2_1/n$ with the following cell parameters $a = 9.4094(10)$ Å, $b = 9.3066(10)$ Å, $c = 20.960(2)$ Å, and $\beta = 99.0375(10)^\circ$. The 3D-X-ray structure of NBQA along with the optimized structure at BPV86/6-311G(d,p) level of theory are depicted in Fig. 2 (a) and (b), respectively. The selected bond lengths, bond angles, and dihedral angles are listed in Tables S1, S2, and S3 (see supplementary material), respectively. The compound contains two planar rings connected by a hydrazide moiety. The first one is the nitrobenzene ring (N4, O3, O4, C13–C18) and the second is the quinoline which is composed of two rings (N1, C1–C9). The two aromatic rings of quinoline are fused almost coaxially, with a dihedral angle between their planes of $N1-C9-C4-C5 = 178.91(6)^\circ$. The nitrobenzene and quinoline groups are in an antiperiplanar conformation with experimental torsion angle $C11-C10-O1-C8 = -179.68(1)^\circ$. On the other hand, the hydrazide fragment adopts a fully extended conformation characterized by a nitrogen to nitrogen covalent bond. The dihedral angle between the plane containing the quinoline moiety and the plane formed by the nitrophenyl ring is $17.48(2)^\circ$, which indicates that the two moieties are almost coplanar. The

ethyl group C–C bond lengths are in the range 1.5083 (13) – 1.5232 (13) Å and are consistent with previously reported values [41]. The C8–O1 bond length [1.376 (1) Å (X-ray) and 1.366, 1.364 Å (BPV86, PBE)] is notably shorter than the normal C–O single bond [1.427 Å] [42] due to the conjugation. The C10–O1 bond length [1.419 (1) Å (X-ray) and 1.436, 1.433 Å (BPV86, PBE)] is normal for the C–O single bond. The deviation of the bond length values for C8–O1 = 1.376 (15), N2–N3 = 1.387 (15), and C11–N2 = 1.344 (19) Å from the standard values which can be attributed to the Sp² hybridization of the quinoline and benzene rings. In the crystal structure of NBQA, the C–C bond lengths in the quinoline moiety are observed in the range of 1.3525 (2) – 1.4209 (18) Å [X-ray] and calculated in the range of 1.380 – 1.440 Å [BPV86 and PBE]. The experimental and theoretical bond lengths are consistent with previous works on quinoline containing molecules [43-45]. Likewise, the C11 = O2 bond lengths of 1.2225 (10) Å [X-ray], 1.228 Å [BPV86] and 1.227 Å [PBE] are in good agreement with the standard value [1.20 Å], indicating a double bond character. In the nitro group, the experimental N4–O3 and N4–O4 bond length values are slightly lower than the corresponding theoretical values due to the presence of intermolecular interactions involving oxygen atoms. Additionally, in the title compound, good compatibility was observed between experimental and theoretical bond angles. The C8–O1–C10 and O1–C10–C11 experimental bond angles were found at 115.71 (10) and 111.63 (12)°, respectively. These angles were calculated at (117.45 and 117.44°) and (112.80 and 112.88°) using BPV86 and PBE functionals, respectively. It is always useful to remember that the experimental data are obtained in the solid phase, while computational results are carried out in the gaseous phase for an isolated molecule. Considering the above findings, it can be said that there is a good agreement between experimental and theoretical geometric parameters.

Figure 2

3.3. Supramolecular features and Hirshfeld surface description

In the crystal, O–H···O, C–H···O and N–H···O hydrogen bonds involving the solvent water molecule, and C–H···π interactions (Table 2) link the molecules into a three-dimensional supramolecular architecture. The crystal is constructed of molecular stacks extending along the *b* and *c* axes. The closest centroid-centroid distance between the nitrobenzene group and the quinoline ring of neighboring molecules is 3.553 Å, and between the two nearly parallel quinoline rings is 3.494 Å thus indicating, however, no observed π-stacking interaction between those groups.

Intermolecular interactions are very useful to understand the molecular packing in the crystal. Quantitative information and contribution of each intermolecular interaction are provided using the Hirshfeld surface (HS) and the fingerprint plots. The HS analysis was described by the normalized contact distance (d_{norm}). Three-dimensional d_{norm} surfaces were obtained from X-ray diffraction results by using the equation reported in the literature [46]. The CrystalExplorer 17.5 program [47] was used to draw the 3D-HS map and 2D-fingerprint plot. The generated HS for NBQA is shown in Fig. 3(a). In this figure, the d_{norm} surfaces are mapped from -0.5332 to 1.3126 Å and the close-contact interactions are indicated by the large and deep red spots. These spots are associated to the weak O–H···O, C–H···O, and N–H···O intermolecular interactions responsible for the hydrogen bonding in the crystal.

The 2D fingerprint plot is displayed in Fig. 3(b) based on d_e and d_i distances from 0.6 to 2.8 Å. As shown in Figure 3(b), the H···H contacts are the most important ones on the surface with a contribution of 32.1% to the HS of NBQA. Other significant contributions are highlighted in Fig. 3(b).

Figure 3

Table 2

3.4. Spectroscopic characterization

3.4.1. Vibrational analysis

IR spectroscopy has always been a real tool to find vibrational modes and recognize the functional groups in organic compounds. NBQA was characterized by FTIR and vibrational frequencies were calculated using BPV86 and PBE functionals with 6-311G (d,p) basis set. The NBQA molecule consists of 43 atoms and hence it shows 123 normal modes of vibrations, from 3500 to 15 cm^{-1} , of which the strongest absorption mode is observed at 2903 cm^{-1} , and the weakest one is observed at 405 cm^{-1} . The observed FTIR modes with their relative intensities, computed frequencies, and assignments are collected in Table S4 (see supplementary material). The experimental FTIR spectrum of NBQA recorded between 400 and 4000 cm^{-1} and simulated IR spectrum using BPV86/6-311G (d,p) and PBE/6-311G (d,p) methods are displayed in Fig. 4(a). The potential energy distribution (PED) for each normal mode was calculated. Due to the overestimation from the experimental values of the DFT calculation, the recommended set of transferable scale factors [48] was used to refine the scale factors. Therefore, the estimated scaling factors for the main vibrational modes were derived as follows: ~ 1.0074 for $\nu(\text{C-H})$, 1.065 for $\nu(\text{N-H})$, and ~ 0.9363 for $\nu(\text{O-H})$ [49-51]. As can be

seen in Fig. 4 and from Table 6, the vibration mode 123 is related to the O–H stretching vibration. This vibration was observed at 3500 cm^{-1} justifying the presence of water molecule in the structure of our compound. The $\nu(\text{OH})$ vibration wavenumbers were calculated using BPV86 and PBE functionals, and the corresponding scaled values are 3500 and 3506 cm^{-1} , respectively. To well compare the vibrational frequencies, the correlation graph showing the calculated wavenumbers (obtained by BPV86/6-311G(d,p) method) versus the experimental ones is plotted in Fig. 4(b). The correlation value $R^2 = 0.9997$ confirmed the good agreement between calculated and experimental frequencies.

Figure 4

Nitro group vibrations

NO_2 stretching vibrations are the most characteristic bands in the IR spectra of aromatic compounds with nitro moiety in their structures. These vibrations vary between symmetric ($\nu_s(\text{NO}_2)$) and asymmetric ($\nu_{as}(\text{NO}_2)$) stretching vibrations with strong absorption intensities. $\nu_{as}(\text{NO}_2)$ and $\nu_s(\text{NO}_2)$ stretching vibrations appeared in the range 1570 – 1485 and 1370 – 1320 cm^{-1} , respectively [52]. In our study, $\nu_{as}(\text{NO}_2)$ and $\nu_s(\text{NO}_2)$ stretching vibrations are observed at 1504 cm^{-1} and 1338 cm^{-1} , respectively. The corresponding theoretical values appeared at 1497 cm^{-1} (BPV86) and 1507 cm^{-1} (PBE) for $\nu_{as}(\text{NO}_2)$ stretching vibration, and 1337 cm^{-1} (BPV86) and 1338 cm^{-1} (PBE) for $\nu_s(\text{NO}_2)$ stretching vibration.

Carbonyl group vibrations

The stretching vibrations of carbonyl ($\text{C}=\text{O}$) are expected in the frequency range 1870 – 1540 cm^{-1} [53]. In the present investigation, the corresponding FTIR band is observed at 1671 cm^{-1} , and the computed values are 1690 cm^{-1} using BPV86/6-311G (d,p) and 1700 cm^{-1} using GGA-PBE/6-311G(d,p) with a contribution of 63 %. The DFT computed values are found to be very close to the experimentally observed value.

C–H and N–H vibrations

In aromatic compounds, the C–H stretching vibrations are identified between 3100 and 3000 cm^{-1} [54]. For NBQA, the $\nu(\text{C–H})$ vibrations are observed at 3093 and 3174 cm^{-1} . As detailed in Table S4 (see supplementary material), these vibrations are calculated in the regions 3174 – 3010 cm^{-1} and 3179 – 3023 cm^{-1} using BPV86/6-311G(d,p) and GGA-PBE/6-311G(d,p) functionals, respectively. It is also well known that in-plane and out-of-plane C–H bending

vibrations occur in the ranges 1300–1000 cm^{-1} and 1000–750 cm^{-1} , respectively [55]. The C–H bending vibrations appear at 1257–1082 cm^{-1} for the in-plane vibration modes and at 850 cm^{-1} for the out of plane vibration modes. These vibrations are also computed at 1257–1002 cm^{-1} [1262–1086 cm^{-1} using PBE functional] and 851 cm^{-1} , respectively. For the $\nu(\text{N–H})$ vibration modes of the amide group, symmetric stretching vibrations appear as a strong broad bands in the region 3500–3300 cm^{-1} [56]. In the present study, the N–H stretching vibration, with a PED of 53%, is found at 3462 cm^{-1} in the FT-IR spectrum. According to the DFT calculations, the values of this mode are 3463 and 3362 cm^{-1} calculated using BPV86 and PBE functionals, respectively. Furthermore, the NNH deformation band [$\delta(\text{NNH})$], with a PED of 54%, is observed at 1545 cm^{-1} in the FT-IR spectrum. The corresponding theoretical wavenumbers are found to be 1545 and 1549 cm^{-1} computed using BPV86 and PBE levels, respectively.

C–C vibrations

As reported previously, the vibrational wavenumbers in the region 1600–1400 cm^{-1} are attributed to the C–C stretching vibrations [57]. Therefore, the C–C stretching vibrations for the title compound are found at 1587 and 1430 cm^{-1} in the FT-IR spectrum. These modes are confirmed by their PED values, which are presented in Table S4 (see supplementary material). The associated theoretical values are calculated in the range of 1585–1437 cm^{-1} and 1590–1439 cm^{-1} using BPV86/6-311G(d,p) and GGA-PBE/6-311G(d,p) functionals, respectively. As can be noted, both of the experimental and theoretical vibrational spectra are in good agreement.

CH₂ group vibrations

The bands corresponding to CH₂ groups can be observed between 3000 and 2865 cm^{-1} [58]. In our research work, the six vibration modes of the CH₂ group were easily assigned. The experimental symmetric and asymmetric stretching vibrations are observed at 2916 cm^{-1} . The corresponding theoretical stretching vibrations are predicted in the range 2955–2951 cm^{-1} and 2923–2903 cm^{-1} using BPV86/6-311G(d,p) and GGA-PBE/6-311G(d,p) functionals, respectively.

C–N, C=N, and N–N vibrations

For the aromatic compound which contains a hydrazide group, the C–N stretching modes are expected in the range 1300–1100 cm^{-1} [59]. In the present case, the $\nu(\text{C–N})$ vibration band is

observed at 1082 cm^{-1} in the IR spectrum and the corresponding calculated value is 1086 cm^{-1} with both BPV86 and PBE levels and a PED contribution of 21%. This mode is not pure but contains a significant contribution from in-plane C–H mode. Usually, the vibrational modes in the region $1650\text{--}1550\text{ cm}^{-1}$ are assigned to the stretching vibration bands of C=N [60]. For NBQA, the observed frequency at 1590 cm^{-1} in the FTIR spectrum is attributed to C=N stretching vibrations. The theoretical $\nu(\text{C}=\text{N})$ stretching mode appears at 1598 and 1605 cm^{-1} computed with BPV86 and PBE levels of theory, respectively. According to the above results, a good correlation between calculated and experimental values for this mode is noted. For the N–N stretching vibrations, in the hydrazide fragment, this mode was calculated at 1172 cm^{-1} using the B3LYP/6-31++G(d,p) method [61]. In the present vibrational analysis, this vibration mode was observed at 1112 cm^{-1} in the IR spectrum and was identified at 1113 and 1123 cm^{-1} by BPV86 and PBE levels of calculations, respectively, with a PED contribution about 32%.

Quinoline and phenyl ring vibrations

In NBQA, in addition to C-H bond, quinoline and phenyl aromatic rings are formed by C=C, C–C, and C–N bonds. The C=C stretching vibrations have been observed at 1671 , 1587 , and 1504 cm^{-1} . These stretching vibrations have been also calculated at 1621 , 1585 , and 1491 cm^{-1} with the PED contributions of 38%, 53%, and 22%, respectively. The C–C stretching vibrations in aromatic compounds, in general, appear in the region of $1650\text{--}1430\text{ cm}^{-1}$ [62]. In the NBQA compound, for both quinoline and phenyl rings, these vibrations are observed at 1590 , 1587 , 1504 , 1430 , and 1300 cm^{-1} in the FT-IR spectrum. The theoretically estimated values are 1598 , 1585 , 1497 , 1437 , and 1288 cm^{-1} with BPV86/6-311G(d,p). The corresponding PBE frequencies are close to experimental and BPV86 values. For the $\nu(\text{C}-\text{N})$ vibration bands of the quinoline ring, the stretching vibrations are well explained in the above C-N vibrations section. These vibrations are observed at 1082 cm^{-1} and calculated at 1086 cm^{-1} . In the quinoline ring, for the C-H in-plane bending vibrations the usual region is $1000\text{--}1300\text{ cm}^{-1}$ in which peaks with strong and weak intensity are observed [63]. In the case of the present study, the C-H in-plane bending vibrations arise as weak bands at 1257 and 1112 cm^{-1} . The calculated values are 1257 and 1113 cm^{-1} with BPV86 functional, and 1262 and 1123 cm^{-1} with PBE functional. The C-H out-of-plane bending vibrations occur in the region of $700\text{--}900\text{ cm}^{-1}$ [64]. The C-H out-of-plane bending vibration of NBQA arises as a peak with medium intensity at 748 cm^{-1} . The calculated values are 749 and 751 cm^{-1} with BPV86 and

PBE functionals, respectively. On the other hand, the bands occurring at 850, 688, and 468 cm^{-1} (814, 663, 499 cm^{-1} with BPV86 and 815, 665, 496 cm^{-1} with PBE using 6-311G (d,p) basis set) are assigned to CCC in-plane bending modes.

3.4.2. ^1H and ^{13}C NMR spectral analysis

The combination of theoretical and experimental nuclear magnetic resonance (NMR) methods has become an adequate possibility to obtain faithful structural results. The NMR spectroscopy was always used as an efficient tool for the determination of molecular structures of organic compounds. The theoretical isotropic chemical shifts of ^1H and ^{13}C NMR for NBQA were obtained using the gauge-independent atomic orbital (GIAO) method with respect to tetramethylsilane (TMS) using the BPV86/6-311G(d,p) level of theory with chloroform as a solvent and the results are summarized in Table S5 (see supplementary material). The corresponding experimental chemical shift values are also presented in the same table. The experimental and theoretical NMR spectra are shown in Fig. S1 (see supplementary material). It should be noted that the TMS shieldings calculated values by BPV86/GIAO/6-311G(d,p) are 31.59 ppm and 183.80 ppm for ^1H and ^{13}C NMR, respectively.

As can be seen from ^1H -NMR results reported in Table S5 (see supplementary material), throughout the molecule, protons give resonance experimentally in the range 4.99-12.49 ppm. Generally, the aromatic protons show chemical shifts at the range of 7.00-8.00 ppm [65]. However, the chemical shifts can be affected by the proton electronic environment. As expected, the CH protons of quinoline and phenyl rings of NBQA generate resonance in the range 7.33-8.96 ppm. The corresponding values were computed in the interval 7.25-9.05 ppm and appear as a multiplet. ^1H -NMR experimental spectroscopy data also show that NH proton gives resonance at a higher value (12.49 ppm) due to the electronegative character of N atom. This value is calculated at 14.71 ppm. In this investigation, CH_2 (H10a and H10b) protons generate resonance at 4.99 ppm. This large value is directly related to the coordination of the electronegative oxygen atom and the two protons of the CH_2 group are in the same environment. Likewise, the theoretical ^1H chemical shift value for CH_2 protons is calculated to be 4.81 ppm with BPV86/6-311G(d,p) level. According to the above results, experimental and theoretical ^1H -NMR chemical shifts are in good agreement.

In the ^{13}C -NMR spectra of NBQA, the quinoline and phenyl carbons resonated at the range 114.88–165.76 and 123.92–165.01 ppm, respectively. The calculated chemical shifts of these

two rings are in the range 112.536–158.745 and 127.663–152.738 ppm. Literature reported that the chemical shift range of aromatic carbon atoms in organic molecules is generally greater than 100 ppm [66]. The chemical shifts of C8 and C16 carbon atoms exhibit the highest values because they are directly linked to oxygen atoms which are known for their large electronegativity. The carbon to which the carbonyl group is attached has the highest chemical shift value and generates resonance at 176.44 ppm. The corresponding calculated value is 164.298 ppm at the BPV86 level by using the GIAO method. The ^{13}C -NMR experimental spectrum exhibits the presence of a peak with the lowest chemical shift value at 71.44 ppm (72.651 ppm with BPV86/6-311G(d,p)) due to the resonance of the methylene carbon atom C10. The carbon atom of the methine group (C12) shows a signal at 148.99 ppm. Furthermore, the chemical shift of the C12 atom is calculated in the high resonance region with a value of 147.089 ppm due to the effect of the imino group (C=N).

3.5. Electronic properties

3.5.1. Frontier molecular orbital (FMO) analysis

The highest occupied molecular orbital (HOMO) and the lowest unoccupied molecular orbital (LUMO) constitute the frontier molecular orbitals (FMOs). Moreover, it is well known that FMOs are involved in the optical properties of materials [67]. Thus, the electron affinity of a molecule is measured by its LUMO energy, while the ionization potential is directly related to the HOMO energy value. The difference between HOMO and LUMO gives the energy band-gap which helps investigate the stability and chemical activity of a molecule [68]. The 3D plot of FMOs determined using the BPV86/6-311G(d,p) method for NBQA is depicted in Fig. 5. As highlighted by Fig. 5, the HOMO is localized over the whole molecule except the nitro group whereas the LUMO density is concentrated on nitrobenzene, hydrazide, and carbonyl fragments. The present HOMO-LUMO analysis reveals that the charge transfer occurs from quinoline moiety to the nitro-phenyl group. The energy values for HOMO, LUMO, and band-gap calculated at BPV86 and PBE functionals with 6-311G(d,p) are listed in Table 3. The energy gap (HOMO–LUMO) values are 2.1336 and 2.1624 eV obtained using BPV86 and PBE functionals, respectively. The BPV86 method has the lowest energy gap values compared to those calculated by other methods [22]. The small energy gap values indicate that the NQBA molecule is more reactive and can be very promising for NLO applications.

Figure 5

3.5.2. UV-Vis spectra

TD-DFT calculations were performed for ten excited states using BPV86/6311G (d,p) level of theory with the non-polar chloroform solvent to obtain the most important electronic transitions in terms of their oscillator strengths and excitation energies of NBQA. The implicit conductor-like polarizable continuum model (CPCM) was used to simulate the solvent effects [69]. The calculated absorption wavelengths (λ), oscillator strengths (f) and excitation energies (E) are given in Table 4 along with their assignments and contributions. The experimental and theoretical UV-Vis spectra of NBQA are shown in Fig 6(a). The UV-Visible spectrum of NBQA is measured in deuteriochloroform solvent. In the present analysis, the significant contributions of the HOMO–LUMO transitions were obtained using the Gauss-Sum 2.2 software [70] based on TD-DFT results. The electronic absorption depends on the transition from the ground to the first excited states and is principally described by the excitation of electrons from the HOMO to the LUMO. The simulated absorption spectrum of NBQA consists of intense transition bands (by TD-DFT with the BPV86 level) at 572.79, 458.47, 456.65 and 373.95 nm with oscillation strengths 0.0116, 0.4740, 0.0197 and 0.0573, respectively. These transitions correspond to 43%, 78%, 96% and 34% contributions from HOMO to LUMO, HOMO–1 to LUMO, HOMO–2 to LUMO and HOMO–1→LUMO+1, respectively, with a charge transfer character from electron-donor (HOMO) to electron-acceptor (LUMO). From the results of Table 4 and as can be seen in Fig. 6(a), the absorption peak observed at 374 nm ($f = 0.0573$) indicates good agreement with the measured experimental wavelength of 372 nm. This electronic absorption corresponds to the transition from the ground state to the eighth excited state and is mainly described by excitation from HOMO–1 to LUMO+1 and HOMO to LUMO+1 with 34% and 57% contributions, respectively. All of these bands are attributed to the combination of $n \rightarrow \pi^*$ and $\pi \rightarrow \pi^*$ transitions. The total density of states (TDOS) provides the character of the molecular orbitals and demonstrates their compositions [71]. The DOS diagram obtained at the BPV86/6-311G(d,p) method for NBQA is plotted in Fig. 6(b). In the TDOS drawing, the red and green lines designate the virtual and occupied orbitals, respectively. Commonly, the DOS diagram occurs from the simultaneous effect of donor and acceptor groups on the electron delocalization.

Table 4

Figure 6

3.6. Global reactivity descriptors and thermodynamic parameters

As mentioned in several research works, the stability of organic molecules can be described by using calculated chemical hardness and softness parameters [72, 46]. Moreover, soft molecules were found to be more polarizable than the hard ones due to their small energy for excitation[73]. In this perspective, the global chemical reactivity descriptors (GCRD) for a molecule are calculated utilizing HOMO and LUMO energy values. The theoretical GCRD parameters of compounds such as electronegativity (χ), chemical hardness (η), chemical potential (P), chemical softness (S), and electrophilicity index (ω) are obtained using the following equations [74]:

$$\chi = \left(\frac{I+A}{2}\right), \eta = \left(\frac{I-A}{2}\right), P = -\left(\frac{I+A}{2}\right), S = \frac{1}{2\eta}, \omega = \frac{\mu^2}{2\eta}$$

where $I = -E_{HOMO}$ and $A = -E_{LUMO}$ are the ionization potential and electron affinity, respectively. The GCRD parameters were evaluated by using BPV86 and GGA-PBE functionals with 6-311G(d,p) basis set and the computed values are gathered in Table 3. The Ionization potential (I) and an electron affinity (A) of the title compound calculated by BPV86 and GGA-PBE levels are 5.7676, 5.6574 eV and 3.6340, 3.4940 eV, respectively. The chemical hardness (η) is one of the most important parameters used to indicate that the charge transfer occurs within a molecule. The values of this parameter obtained with BPV86/6-311G(d,p) and GGA-PBE/6-311G(d,p) are 1.0668 and 1.0812, respectively. Besides, the molecular stability of the title compound can be explained by the negative values of the chemical potential (P) (-4.7008 and -4.5762) obtained with BPV86 and GGA-PBE functionals. Whereas, the chemical reactivity of the title molecule is measured by its softness which has low values (0.4687 and 0.4625) obtained with BPV86 and GGA-PBE functionals. The values of selected thermodynamic parameters of the title compound at 298.15 K in the ground state are obtained from the calculated harmonic frequencies. These parameters are estimated using BPV86 and GGA-PBE functionals with the 6-311G(d,p) basis set and are summarized in Table 3. As can be seen in the table, the variation in zero-point vibrational energies calculated using BPV86 functional is lower than the corresponding value obtained from the PBE functional. Whereas, no changes were noticed for the other thermodynamic parameters using both functionals.

Table 3

3.7. Reduced Density Gradient (RDG) analysis

To explore intra and inter non-bonded interactions in a molecular system, the reduced density gradient (RDG) is used. The regions of these interactions and their graphical visualization are

provided by using the RDG analysis based on the electron density and its derivatives [75, 76]. The RDG is given by the following equation:

$$RDG(r) = \frac{1}{2(3\pi r^2)^{1/3}} \frac{|\nabla\rho(r)|}{\rho(r)^{4/3}}$$

where $\rho(r)$ is the electron density and $\nabla\rho(r)$ is the gradient of $\rho(r)$ at the point r . The graphical representation of $\rho(r)$ versus $\text{sign}(\lambda_2)\rho$, where $\text{sign}(\lambda_2)\rho$ is the second eigenvalue of the electron density, provides useful information regarding the strength and nature of the interactions. The value and sign of $\text{sign}(\lambda_2)\rho$ are used to explain the nature of interactions. The repulsive, attractive and Van der Waals (VDW) interactions correspond to $\text{sign}(\lambda_2)\rho > 0$, $\text{sign}(\lambda_2)\rho < 0$ and $\text{sign}(\lambda_2)\rho \approx 0$, respectively. The 2D scatter plot and the 3D RDG isosurface densities of NBQA are shown in Fig. 7. As can be seen in Fig. 7, red region indicates strong repulsive interactions mainly observed in centers of quinoline and aromatic rings, blue region indicates strong attractive interactions corresponding to the strong hydrogen bonds $N_2-H\cdots O_w$ and $O_w-H\cdots N_1$, and the green region can be identified as intermediate interactions or VDW weak attractive interactions due to $H\cdots H$ interaction. On the other hand, the strong steric effect is indicated by the red color. RDG analysis confirms the previous results obtained by the HS analysis to identify interacting regions in the molecular packing of NBQA.

Figure 7

3.8. Molecular electrostatic potential analysis

The molecular electrostatic potential (MEP) and the total electron density are two important parameters to identify regions responsible for hydrogen bonding interactions [77] as well as potential electrophilic and nucleophilic sites in the molecule [78]. In addition, the charge distributions of molecules are illustrated using the MEP surfaces. The knowledge of these distributions can be used to investigate the nature of the chemical bonds and how molecules interact with one another. The MEP can be defined at a given point $r(x,y,z)$ in the space around a molecule (in atomic units) by the following equation:

$$V(r) = \sum_A \frac{Z_A}{|R_A - r|} - \int \frac{\rho(r')}{|r' - r|} dr'$$

where Z_A is the charge on nucleus A located at R_A and $\rho(r)$ is the electron density. The first term in the expression represents the effect of the nuclei and the second characterizes that of electrons. $V(r)$ is a real physical property which can be determined by X-ray diffraction experiment or theoretical methods [79,80]. The 3D MEP for the title compound was calculated by using BPV86/6-311G(d,p) level and the corresponding plot is shown in Fig. 8.

Electrostatic potential correlates with sites of chemical reactivity of the molecule. Thus, the positive regions of the MEP picture with the blue colour are related to nucleophilic reactivity and the negative regions with the red colour indicate sites for electrophilic reactivity [81]. In Fig. 8, the negative regions are mainly located over the nitro group and carbonyl O2 atom, whereas the positive region, is more concentrated on hydrogen atoms indicating a possible site for nucleophilic attack.

Figure 8

3.9. Population charge analysis

3.9.1. Natural bond orbital (NBO)

Natural bond orbital (NBO) analysis is defined as a potent method for investigating molecular packing insured by intra and inter-molecular interactions. At the same time, NBO analysis helped in understanding the stability of the molecule arising from hyper-conjugative interaction, stabilization energy, and charge transfer in the molecular system by utilizing a second-order perturbation approach [82, 83]. In this context, all possible interactions including different types of donor-acceptor and their stabilization energies in the NBO basis can be evaluated by using the second-order Fock-matrix [84]. The stabilization energy ($E^{(2)}$) related to the delocalization from the donor (i) to the acceptor (j) is evaluated using the following equation:

$$E^{(2)} = \Delta E_{ij} = q_i \frac{F_{(i,j)}^2}{\varepsilon_j - \varepsilon_i}$$

Where q_i is the donor orbital occupancy; ε_j and ε_i are the diagonal elements and $F_{(i,j)}$ is the off-diagonal NBO Fock-matrix element. For the most strong hyperconjugative interactions, the parameters such as electron density (ED), donors and acceptors, stabilization energy ($E^{(2)}$), energy difference ($\varepsilon_j - \varepsilon_i$) and polarization energy $F(i, j)$ obtained using BPV86/6-311G(d, p) method are displayed in Table 5. The high $E^{(2)}$ value indicates the more intensive interaction between electron donors and acceptors [85]. The results in the gas phase showed that the strongest interactions ($n \rightarrow \pi^*$) are from the lone pair of electrons $n_3(O4)$ to the antibonding orbitals $\pi^*(N4-O3)$ with the stabilization energy of $158.99 \text{ kcal.mol}^{-1}$. The intramolecular hyperconjugative interactions of π (C1-N1) orbital to π^* (C2-C3) and π^* (C4-C9) leading to stabilization energy of 10.40 kJ/mol and 18.59 kJ/mol, respectively. In the same way, the case of π (C16-C17) orbital to π^* (N4-O3) shows strong stabilization energy of 32.11 kJ/mol. Furthermore, the NBO analysis shows that the antibonding orbitals- $\pi^*(C1-N1)$, $\pi^*(C4-C9)$, $\pi^*(C7-C8)$, $\pi^*(C12-N3)$ and $\pi^*(C16-C17)$ NBO's conjugate with $\pi^*(C4-C9)$,

$\pi^*(C5-C6)$, $\pi^*(C5-C6)$, $\pi^*(C13-C18)$ and $\pi^*(C14-C15)$ leading to the enormous stabilization energies of 133.87, 141.13, 168.97, 146.44 and 171.53 kcal/mol respectively.

Table 5

3.9.2. Atomic charges

Atomic charge calculations are helpful to quantify the electronic structure changes due to atomic displacements and can be used to explain the changes in molecular properties like nonlinear optical properties [86]. The atomic charge values calculated by Mulliken and natural bond orbital (NBO) analysis for NBQA at the BPV86 functional with the 6-311G(d,p) basis set are summarized in Table 6. The better represented graphical configuration of our results is illustrated in Fig. S2 (see supplementary material). According to the NBO and Mulliken results, all of the hydrogen atoms are positively charged. In the NBQA molecule, the Hw2, Hw1 and H atoms have high positive NBO charges 0.492, 0.465 and 0.422 e, and Mulliken charges 0.313, 0.265 and 0.291 e, respectively. These charges are important compared to the other hydrogen atoms due to the electronegative character of the Ow and N2 atoms. The presence of intra and inter-molecular hydrogen bonding in the crystal packing is indicated by the large positive charge values of hydrogen atoms. On the other hand, the oxygen and nitrogen atoms, namely, Ow, O1, O2, O3, O4, N1, N2 and N3 have the most negative charges in the title molecule. The carbon atoms C1, C8, C9, C11, C12 and C16 bounded to the N1, N2, N3, N4, O1 and O2 atoms have positive charges due to the electron-withdrawing nature of nitrogen and oxygen atoms. The calculated NBO and Mulliken charges using BPV86/6-311G(d,p) level of theory are in good agreement with the molecular electrostatic potential results.

Table 6

3.10. Nonlinear optical activity

Parameters such as dipole moment (μ), polarizability (α) and the first order hyperpolarizability (β) are determined to study the nonlinear optical properties (NLO). In this work, the NLO properties for the title compound were evaluated by using BPV86 and GGA-PBE functionals with 6-311G(d,p) basis set. The μ , α and β are defined as [21]:

$$\mu = (\mu_x^2 + \mu_y^2 + \mu_z^2)^{1/2}$$

$$\alpha = 1/3 (\alpha_{xx} + \alpha_{yy} + \alpha_{zz})$$

$$\beta = (\beta_x^2 + \beta_y^2 + \beta_z^2)^{1/2}$$

Where

$$\beta_x = (\beta_{xxx} + \beta_{xyy} + \beta_{xzz})$$

$$\beta_y = (\beta_{yyy} + \beta_{yxx} + \beta_{yzz})$$

$$\beta_z = (\beta_{zzz} + \beta_{zxx} + \beta_{zyy})$$

The α and β values of Gaussian output are in atomic unit (a.u.), therefore they were converted into electrostatic unit (esu) (for α ; 1 a.u. = 0.1482×10^{-24} esu and for β ; 1 a.u. = 8.6393×10^{-33} esu).

In the gas phase, the calculated NLO properties for the title compound are summarized in Table 7. The molecular dipole moment values are 13.67 and 13.54 D for BPV86 and GGA-PBE levels, respectively. The molecular polarizability (α_0) values are equal to 44.97×10^{-24} and 44.85×10^{-24} esu for BPV86 and GGA-PBE levels, respectively. It is clearly observed from Table 7, the β values in the gas phase, calculated with BPV86 and GGA-PBE functionals, are 56.68×10^{-30} (293 times that of urea [87]) and 55.98×10^{-30} esu (290 times that of urea), respectively. In addition, the most important obtained value for β in the gas phase is comparable with other NLO compounds as shown in Figure 9. Therefore, all these results predict that the title compound could be a potential candidate for future researches of nonlinear optical properties.

As the NLO properties are affected by the environment [88], the molecular dipole moment, the polarizability and the first order hyperpolarizability were computed by considering the polarizable continuum model (PCM) [89,90] at the same level of theory and using solvents found in Gaussian program (CCl₄, diethylether, chloroform, acetone, ethanol, acetonitrile, DMSO and water). The NLO parameters along with HOMO-LUMO energy gap for the title compound were calculated and listed in Table 7. As can be seen from this table, the BPV86 method gives meaningful results compared to the PBE method. On the other hand, with increasing solvent polarity, NLO properties for the title molecule are increasing and HOMO-LUMO energy gap is decreasing. These conclusions confirm the results of previously published work on NLO materials which concluded that BPV86 gives accurate results compared to the other DFT functionals [22].

Figure 9

Table 7

4. Conclusion

In the current work, a novel quinoline derivative (E)-N'-(4-nitrobenzylidene)-2-(quinolin-8-yloxy) acetohydrazide monohydrate (NBQA) was synthesized and investigated by using single crystal X-ray

diffraction, spectroscopic (FT-IR, NMR and UV-Vis) analysis. NBQA crystal belongs to the monoclinic crystal system with space group $P2_1/n$. Furthermore, the geometry optimization and vibrational frequencies were obtained by theoretical calculations based on DFT method using both BPV86 and GGA-PBE functionals with 6-311G(d, p) basis set. Conformational analysis for NBQA was accomplished, and the most stable conformer was selected. Structure elucidation using NMR, IR, X-ray crystallography, and other spectroscopic techniques is a challenging field of research. With technical progress, data analysis and spectral interpretation became the most certain way of structural elucidation. In this context, prediction of ^1H and ^{13}C NMR chemical shifts and vibration frequencies by DFT computation have been demonstrated to be a viable strategy for the determination of the molecular structure and the relative configuration of new molecules. In addition, computations of UV/Vis spectra using DFT method with the appropriate basis set have been central to the elucidation of the electronic structure of NBQA. According to this study, the experimental and theoretical structural parameters are in good agreement. A good linearity between calculated and experimental vibration frequencies was also observed. In the crystal packing, molecules were linked into 3D-network by $\text{C-H}\cdots\text{O}$ and $\text{N-H}\cdots\text{O}$ intermolecular interactions responsible for the hydrogen bonding. These interactions have been studied using HS and fingerprint tools displaying that the major contributions are $\text{H}\cdots\text{H}$ contacts with 32.1%. The UV-Visible characterization of NBQA in deuteriochloroform solvent was performed in which experimental and TD-DFT spectra reveal that absorption bands are related to $n\rightarrow\pi^*$ and $\pi\rightarrow\pi^*$ electronic transitions. Donor and acceptor groups effect on the electron delocalization was highlighted based on the DOS diagram. The GCRD parameters obtained using the same levels of theory with the help of HOMO-LUMO band gap indicate that the title molecule has high kinetic stability explained by the negative values of the chemical potential and lower chemical reactivity. The thermodynamic parameters are also calculated. The energy band gap values between HOMO and LUMO levels were found to be 2.1336 and 2.1624 eV obtained using BPV86 and PBE functionals, respectively. These energies confirm that the charge transfer occurs within the title molecule and it can be very promising for NLO applications. The reduced density gradient (RDG) approach allowed to analyze the weak attractive interactions, strong attraction, and steric repulsion existed in the title compound. On the other hand, hyperconjugation interactions and stabilization energies were displayed using NBO calculation. The MEP drawing showed that the electronegative atoms of nitro and carbonyl groups represent the most negative potential sites and the hydrogen atoms are the most positive potential sites. These sites provide details about the possible regions for inter- and intramolecular hydrogen bonding. Moreover, a complete NLO analysis was carried out using the most known solvents. This analysis allowed us to obtain the molecular dipole moment, the average polarizability, and the first-order hyperpolarizability. NLO results indicate that the title molecule has a good β value (56.68×10^{-30} esu in the gas phase which is 293 times that of urea) compared to the other known compounds in the field. In addition, the decrease

in the HOMO-LUMO energy gap and the increase in solvent polarity were accompanied by an increase in the hyperpolarizability values.

Supplementary crystallographic data

Crystallographic data for the structure reported in this article have been deposited with Cambridge Crystallographic Data Center, CCDC 2006263. Copies of this information may be obtained free of charge from the Director, CCDC, 12 Union Road, Cambridge, CB2 1EZ, UK. Facsimile (44) 01223 336 033, E-mail: deposit@ccdc.cam.ac.uk or <http://www.ccdc.com.ac.uk/deposit>.

Declaration of interests

None

Acknowledgments

The authors gratefully acknowledge the financial support via PRFU project from The Algerian Ministry of Higher Education and Scientific Research, the Directorate General of Scientific Research and Technological Development (DGRSDT), and Abdelhamid Ibn Badis University of Mostaganem.

References

- [1] L. Srikanth, N. Raghunandan, P. Srinivas, G. A. Reddy, Synthesis and evaluation of newer quinoline derivatives of thiazolidinediones for their antidiabetic activity, *Int. J. Pharm. Bio. Sci.* 1 (2010) 120–131.
- [2] E. Pitta, O. Balabon, M. K Rogacki, J. Gomez, F. Cunningham, J. Joosens, K. Augustyns, P. Veken, R. Bates, Differential characterization using readily accessible NMR experiments of novel N- and O-alkylated quinolin-4-ol, 1,5-naphthyridin-4-ol and quinazolin-4-ol derivatives with antimycobacterial activity, *Eur. J. Med. Chem.* 125 (2017) 890–901.
- [3] A. Koul, E. Arnoult, N. Lounis, J. Guillemont, K. Andries, The challenge of new drug discovery for tuberculosis, *Nature* 469 (2011) 483–490.
- [4] A. Marella, O. P. Tanwar, R. Saha, M. R. Ali, S. Srivastava, M. Akhter, M. Shaquiquzzaman, M. M. Alam, Quinoline: A versatile heterocyclic, *J. SPJ Off. Publ. Saudi Pharm. Soc.* 21 (2013) 1–12.
- [5] M. Gyoten, H. Nagaya, S. Fukuda, Y. Ashida, Y. Kawano, Synthesis of eosinophil infiltration inhibitors with antihistaminic activity, *Chem. Pharm. Bull.* 51 (2003) 122–133.
- [6] A. G. Mac Diarmid, A. J. Epstein, Application of thin films of polyaniline and polypyrrole in novel light-emitting devices and liquid-crystal devices, *J. Am. Chem. Soc. Eds. Ch026* (1997) 395–407.
- [7] A. J. Epstein, Electrically conducting polymers, *Science Technology MRS. Bull.* 22 (1997) 16–23.
- [8] S. Eswaran, A. V. Adhikari, I. H. Chowdhury, N. K. Pal, K. D. Thomas, New quinoline derivatives: synthesis and investigation of antibacterial and antituberculosis properties, *Eur. J. Med. Chem.* 45 (2010) 3374–3383.

- [9] M. C. Mandewale, B. Thorat, Y. Nivid, R. Jadhav, A. Nagarsekar, R. Yamgar, Synthesis, structural studies and antituberculosis evaluation of new hydrazone derivatives of quinoline and their Zn(II) complexes, *J. Saudi Chem. Soc.* 22 (2018) 218–228
- [10] O. Tamer, D. Avci, Y. Atalay, The effects of electronegative substituent atoms on structural, vibrational, electronic and NLO properties of some 4-nitrostilbene derivatives *Spectrochim. Acta* 136 (2015) 644–650.
- [11] L. Zhang, A. Fonari, Y. Liu, A.-L. M. Hoyt, H. Lee, D. Granger, S. Parkin, T. P. Russell, J. E. Anthony, J.-L. Brédas, V. Coropceanu, A. L. Briseno, Bistetracene: An air-stable, high-mobility organic semiconductor with extended conjugation, *J. Am. Chem. Soc.* 136 (2014) 9248–9251.
- [12] J.-L. Brédas, J. E. Norton, J. Cornil, V. Coropceanu, Molecular understanding of organic solar cells: The challenges, *Acc. Chem. Res.* 42(11) (2009) 1691–1699.
- [13] S. Yahiaoui, A. Moliterni, N. Corriero, C. Cuocci, K. Toubal, A. Chouaih, A. Djafri, F. Hamzaoui, 2-thioxo-3N-(2-methoxyphenyl)-5-[4'-methyl-3'-N-(2'-methoxyphenyl)thiazol-2'(3'H)-ylidene]thiazolidin-4-one: synthesis, characterization, X-ray single crystal structure investigation and quantum chemical calculations, *J. Mol. Struct.* 1177 (2019) 186–192.
- [14] N. Boukabcha, A. Djafri, Y. Megrouss, Ö. Tamer, D. Avci, M. Tuna, N. Dege, A. Chouaih, Y. Atalay, A. Djafri, F. Hamzaoui, Synthesis, crystal structure, spectroscopic characterization and nonlinear optical properties of (Z)-N'-(2,4-dinitrobenzylidene)-2-(quinolin-8-yloxy)acetohydrazide, *J. Mol. Struct.* 1194 (2019) 112–123.
- [15] R. Rahmani, A. Djafri, J.C. Daran, A. Djafri, A. Chouaih, F. Hamzaoui, Crystal structure of (2Z,5Z)-3-(4-methoxyphenyl)-2-[(4-methoxyphenyl)imino]-5-[(E)-3-(2-nitrophenyl)-allylidene]-1,3-thiazolidin-4-one, *Acta Crystallogr. E: Struct. Rep. Online* 72 (2016) 155–157.
- [16] N. Khelloul, K., Toubal, N. Benhalima, R. Rahmani, A. Chouaih, A. Djafri, F. Hamzaoui, Crystal structure, Hirshfeld surface analysis and computational studies of thiazolidin-4-one derivative: (Z)-5-(4-chlorobenzylidene)-3-(2-ethoxyphenyl)-2-thiothiazolidin-4-one, *Acta Chim. Slov.* 63 (2016) 619–626.
- [17] R. Rahmani, A. Djafri, A. Chouaih, A. Djafri, F. Hamzaoui, R. Rizzi, A. Altomare, Synthesis, molecular and solid state structure of 5-(5-nitro furan-2-ylmethyl)-3-N-(2-methoxy phenyl), 2-N'-(2-methoxyphenyl) imino thiazolidin-4-one: X-ray powder diffraction and DFT studies, *J. Mol. Struct.* 1143 (2017) 259–264.
- [18] A. Djafri, A. Chouaih, J.C. Daran, A. Djafri, F. Hamzaoui, Crystal and molecular structure of (2Z,5Z)-3-(2-methoxyphenyl)-2-[(2-methoxyphenyl)imino]-5-(4-nitrobenzylidene)thiazolidin-4-one, *Acta Crystallogr. E: Struct. Rep. Online* 73 (2017) 511–514.
- [19] K. Toubal, N. Boukabcha, Ö. Tamer, N. Benhalima, S. Altürk, D. Avci, A. Chouaih, Y. Atalay, A. Djafri, F. Hamzaoui, Spectroscopic (FT-IR, ¹H and ¹³C NMR) characterization and density functional theory calculations for (Z)-5-(4-nitrobenzylidene)-3-N(2-ethoxyphenyl)-2-thiothiazolidin-4-one (ARNO), *J. Mol. Struct.* 1147 (2017) 569–581.
- [20] Y. Chen, Y. Liu, Q. Zhang, Y. Yan, W. Yin, Degradation of bromobenzene via external electric field, *J. Theor. Comput. Chem.* 19(1) (2020) 2050004-1–2050004-10.
- [21] R. Rahmani, N. Boukabcha, A. Chouaih, F. Hamzaoui, S. Goumri-Said, On the molecular structure, vibrational spectra, HOMO-LUMO, molecular electrostatic potential, UV-Vis, first order hyperpolarizability, and thermodynamic investigations of 3-(4-chlorophenyl)-1-(1-ylridine-3-yl) prop-2-en-1-one by quantum chemistry calculations, *J. Mol. Struct.* 1155 (2018) 484–495

- [22] A. Eşme, Theoretical investigation on the molecular structure, electronic, spectroscopic studies and nonlinear optical properties of 5-bromo-1-(2-cyano-pyridin-4-yl)-1H-indazole-3-carboxylic acid diethylamide: a DFT and TD-DFT Study, *Acta Phys. Pol. A* 136 (2019) 378–394.
- [23] SAINT, version 8.34A, Bruker, Bruker AXS Inc., Madison, WI, (2013).
- [24] APEX2, version 2014.9-0, Bruker, Bruker AXS Inc., Madison, WI, (2014).
- [25] SADABS, version 2014/4, Bruker, Bruker AXS Inc., Madison, WI, (2014).
- [26] G. M. Sheldrick, A. Short History of SHELX, *Acta Crystallogr. A* 64 (2008) 112–122.
- [27] G. M. Sheldrick, Crystal structure refinement with SHELXL, *Acta Crystallogr. A* 71 (2015) 3–8.
- [28] O. Dolomanov, L. J. Bourhis, R. J. Gildea, J. A. K. Howard, H. Puschmann, OLEX2: a complete structure solution, refinement and analysis program, *J. Appl. Crystallogr.* 42 (2009) 339–341.
- [29] M. J. Frisch, G. W. Trucks, H. B. Schlegel, G. E. Scuseria, M. A. Robb, J. R. Cheeseman, G. Scalmani, V. Barone, B. Mennucci, G. A. Petersson, H. Nakatsuji, M. Caricato, X. Li, H. P. Hratchian, A. F. Izmaylov, J. Bloino, G. Zheng, J. L. Sonnenberg, M. Hada, M. Ehara, K. Toyota, R. Fukuda, J. Hasegawa, M. Ishida, T. Nakajima, Y. Honda, O. Kitao, H. Nakai, T. Vreven, J. A. Montgomery, Jr., J. E. Peralta, F. Ogliaro, M. Bearpark, J. J. Heyd, E. Brothers, K. N. Kudin, V. N. Staroverov, T. Keith, R. Kobayashi, J. Normand, K. Raghavachari, A. Rendell, J. C. Burant, S. S. Iyengar, J. Tomasi, M. Cossi, N. Rega, J. M. Millam, M. Klene, J. E. Knox, J. B. Cross, V. Bakken, C. Adamo, J. Jaramillo, R. Gomperts, R. E. Stratmann, O. Yazyev, A. J. Austin, R. Cammi, C. Pomelli, J. W. Ochterski, R. L. Martin, K. Morokuma, V. G. Zakrzewski, G. A. Voth, P. Salvador, J. J. Dannenberg, S. Dapprich, A. D. Daniels, O. Farkas, J. B. Foresman, J. V. Ortiz, J. Cioslowski, D. J. Fox, Gaussian 09, Revision B.01, Gaussian, Inc., Wallingford CT, (2009).
- [30] S. H. Vosko, L. Wilk, M. Nusair, Accurate spin-dependent electron liquid correlation energies for local spin density calculations: a critical analysis, *Can. J. Phys.* 58 (1980) 1200–1211.
- [31] J.P. Perdew II, Density-functional approximation for the correlation energy of the inhomogeneous electron gas, *Phys. Rev. B* 33(12) (1986) 8822–8822.
- [32] J.P. Perdew, K. Burke, M. Ernzerhof, Generalized gradient approximation made simple, *Phys. Rev. Lett.* 78 (1997) 1396–1396.
- [33] E. Frisch, H. P. Hratchian, R. D. Dennington II, T. A. Keith, J. Millam, B. Nielsen, A. J. Holder, J. Hiscocks. Gaussian, Inc. GaussView Version 5.0.8, (2009).
- [34] M. H. Jamroz, Vibrational Energy Distribution Analysis (VEDA 4) Program, Warsaw, Poland, (2004).
- [35] E. D. Glendening, A. E. Reed, J. E. Carpenter, F. Weinhold, NBO Version 3.1, TCI, University of Wisconsin, Madison, (1998).
- [36] R. E. Stratmann, G. E. Scuseria, M. J. Frisch, An efficient implementation of time-dependent density-functional theory for the calculation of excitation energies of large compounds, *J. Chem. Phys.* 109 (1998) 8218–8224.
- [37] E. Cancès, B. Mennucci, J. Tomasi, A new integral equation formalism for the polarizable continuum model: theoretical background and applications to isotropic and anisotropic dielectrics, *J. Chem. Phys.* 107 (1997) 3032–3041.
- [38] N. M. O'Boyle, A. L. Tenderholt, K. M. Langner, Software news and updates cclib: A library for package-independent computational chemistry algorithms, *J. Comp. Chem.* 29 (2008) 839–845.
- [39] T. Lu, F. Chen, Multiwfn: A multifunctional wavefunction analyzer, *J. Comput. Chem.* 33 (2012) 580–592.

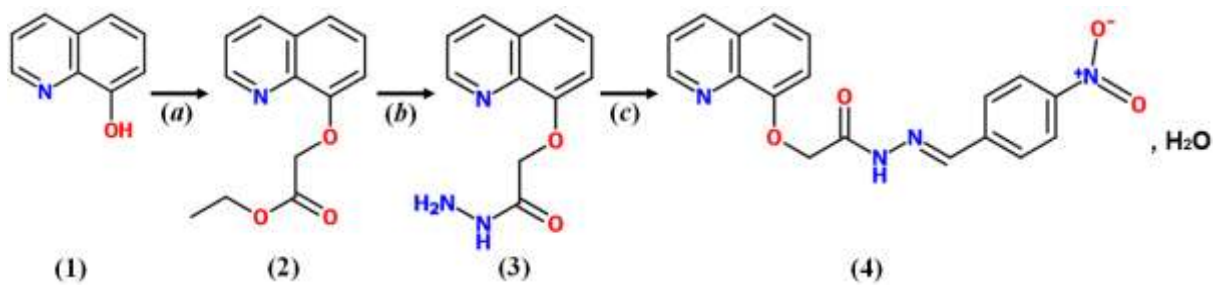
- [40] W. Humphrey, A. Dalke, K. Schulten, VMD: Visual molecular dynamics, *J. Mol. Graph.* 14 (1996) 33–38.
- [41] J. Alshawi, M. Yousif, G. Timco, I. J. Vitorica Yrezabal, R. Winpenny, M. J. Al-Jeboori, Crystal structure of diethyl 3,3'-(2,2'-(1E)-[1,4-phenyl-enebis(azan-1-yl-1-yl-idene)])bis-(methan-1-yl-1-yl-idene)bis-(1H-pyrrole-2,1-di-yl)}di-propano-ate, *Acta Crystallogr. E: Struct. Rep. Online* 71 (2015) o259–o260.
- [42] R. Wan, L.-H. Yin, F. Han, B. Wang, J.-T. Wang, 2-(2,4-Dichloro-phen-yl)-3-[5-(4-methoxy-phen-yl)-1,3,4-thia-diazol-2-yl]-1,3-thia-zolidin-4-one, *Acta Crystallogr. E: Struct. Rep. Online* 64 (2008) o795–o795.
- [43] R. I. Bahoussi, A. Djafri, A. Chouaih, A. Djafri, F. Hamzaoui, Crystal structure and Hirshfeld surface analysis of ethyl 2-([4-ethyl-5-(quinolin-8-yloxymethyl) -4H1,2,4-triazol-3-yl]sulfonyl) acetate, *Acta Crystallogr. E: Struct. Rep. Online* 73 (2017) 173–176.
- [44] A. Cabrera, L. D. Miranda, H. Reyes, G. Aguirre, D. Chavez, Crystal structure of ethyl 2,4-dichloroquinoline-3-carboxylate. *Acta Crystallogr. E: Struct. Rep. Online* 71 (2015) o939–o939.
- [45] V. M. Sunitha, S. Naveen, H. R. Manjunath, S. B. Benaka Prasad, V. Manivannan, N. K. Lokanath, Crystal structure of ethyl 2-(3,5-difluorophenyl)quinoline-4-carboxylate, *Acta Crystallogr. E: Struct. Rep. Online* 71 (2015) o341–o342.
- [46] N. E. H. Belkafouf, F. Triki Baara, A. Altomare, R. Rizzi, A. Chouaih, A. Djafri, F. Hamzaoui, Synthesis, PXRD structural determination, Hirshfeld surface analysis and DFT/TD-DFT investigation of 3N-ethyl-2N'-(2-ethylphenylimino) thiazolidin-4-one, *Journal of Molecular Structure*, 1189 (2019) 8–20.
- [47] M. J. Turner, J. J. MacKinnon, S. K. Wolff, D. J. Grimwood, P. R. Spackman, D. Jayatilaka, M. A. Spackman, *Crystal Explorer 17.5*, University of Western Australia, 2017.
- [48] P. Pulay, G. Fogarasi, G. Pongor, J. E. Boggs, A. Vargha, Combination of theoretical ab initio and experimental information to obtain reliable harmonic force constants. Scaled quantum mechanical (QM) force fields for glyoxal, acrolein, butadiene, formaldehyde, and ethylene, *J. Am. Chem. Soc.* 105 (1983) 7037–7047.
- [49] I. M. Alecu, J. Zheng, Y. Zhao, D. G. Truhlar, Computational Thermochemistry: Scale Factor Databases and Scale Factors for Vibrational frequencies Obtained from Electronic Model Chemistries, *J. Chem. Theory. Comput.* 6 (2010) 2872–2887.
- [50] T. Bardakçı, M. Kumru, S. Guner, Molecular structure, vibrational and EPR spectra of Cu(II) chloride complex of 4-amino-1-methylbenzene combined with quantum chemical calculations, *J. Mol. Struct.* 1054–1055 (2013) 76–82.
- [51] A. C. S. S. Bernardino, A. M. R. Teixeira, J. E. S. A. de Menezes, C. C. C. Pinto, H. S. Santos, P. T. C. Freire, H. D. M. Coutinho, D. M. Sena Junior, P. N. Bandeira, R. Braz-Filho, Spectroscopic and microbiological characterization of labdane diterpene 15,16-epoxy-4-hydroxy-labda-13(16),14-dien-3,12-dione isolated from the stems of *Croton jacobinensis*, *J. Mol. Struct.* 1147 (2017) 335–344.
- [52] O. Tamer, D. Avcı, Y. Atalay, The effects of electronegative substituent atoms on structural, vibrational, electronic and NLO properties of some 4-nitrostilbene derivatives, *Spectrochimica Acta Part A: Molecular and Biomolecular Spectroscopy Part B Spectrochim. Acta* 136 (2015) 644–650.
- [53] B. H. Stuart, *Infrared spectroscopy: fundamentals and applications*, John Wiley & Sons, 2004.
- [54] M. Rafilovich, J. Bernstein, Serendipity and four polymorphic structures of benzidine, $C_{12}H_{12}N_2$, *J. Am. Chem. Soc.* 128 (2006) 12185–12191.
- [55] Ö. Tamer, B. S. Arslan, D. Avcı, M. Nebioğlu, Y. Atalay, B. Çoşut, Synthesis, molecular structure, spectral analysis and nonlinear optical studies on 4-(4-bromophenyl)-1-tert-butyl-3-methyl-1H-pyrazol-5-amine: A combined experimental and DFT approach, *J. Mol. Struct.* 1106 (2016) 89–97.

- [56] G. P. Sheeja Mol, D. Aruldas, I. Hubert Joe, S. Balachandran, Normal coordinate analysis and fungicidal activity study on anilazine and its related compound using spectroscopic techniques, *Chem. phy. lett.* 654 (2016) 125–134.
- [57] T. Polat, F. Bulut, I. Arican, F. Kandemirli, G. Yildirim, Vibrational assignments, spectroscopic investigation (FT-IR and FT-Raman), NBO, MEP, HOMO–LUMO analysis and intermolecular hydrogen bonding interactions of 7-fluoroisatin, 7-bromoisatin and 1-methylisatin – A comparative study, *J. Mol. Struct.* 1101(2015) 189–211.
- [58] F. Chain, E. Romano, P. Leyton, C. Paipa, C. A. N. Catalan, M. A. Fortuna, S. A. Brandan, An experimental study of the structural and vibrational properties of sesquiterpene lactone cnicin using FT-IR, FT-Raman, UV-visible and NMR spectroscopies, *J. Mol. Struct.* 1065-1066 (2014) 160–169.
- [59] M. Silverstein, G. C. Basseler, C. Morill, *Spectrometric identification of organic compounds*, Wiley, New York, 1981.
- [60] G. Socrates, *Infrared, raman characteristic, group frequency*, Third ed., Wiley, 2001.
- [61] S. Guner, Y. Atalay, A. Dolma, Experimental and theoretical study of 4-cyanobenzaldehyde isonicotinoyl-hydrazone monohydrate, *J. Mol. Struct.* 984 (2010) 389–395.
- [62] V. Krishnakumar, N. Surumbakuzhali, S. Muthunatesan, *Spectrochim. Acta A* 71 (2009) 1810–1813.
- [63] N. Puviarasan, V. Arjunan, S. Mohan, FT-IR and FT-Raman spectral investigations on 4-aminoquinoline and 5-aminoquinoline, *Turk J. Chem.* 28 (2004) 53–65.
- [64] N. B. Colthup, L. H. Daly, S. E. Wiberly, *Introduction to infrared and Raman spectroscopy*, Third ed., Academic Press, Boston, 1990.
- [65] N. Subramania, N. Sundaraganesan, J. Jayabharathi, Molecular structure, spectroscopic (FT-IR, FT-Raman, NMR, UV) studies and first-order molecular hyperpolarizabilities of 1,2-bis(3-methoxy-4-hydroxybenzylidene) hydrazine by density functional method, *Spectrochim. Acta A* 76 (2010) 259–269.
- [66] H. O. Kalinowski, S. Berger, S. Braun, *Carbon-13 NMR spectroscopy*, John Wiley & Sons, Chichester, 1988.
- [67] I. Fleming, *Frontier orbitals and organic chemical reactions*, Wiley, London, 1976.
- [68] S. Altürk, D. Avcı, Ö. Tamer, Y. Atalay, 1H-pyrazole-3-carboxylic acid: Experimental and computational study, *J. Mol. Struct.* 1164 (2018) 28–36.
- [69] M. Cossi, N. Rega, G. Scalmani, V. Barone, Energies, structures, and electronic properties of molecules in solution with the C-PCM solvation model, *J. Comput. Chem.* 24 (2003) 669–681.
- [70] N. M. O'Boyle, A. L. Tenderholt, K. M. Langner, Software news and updates cclib: A Library for Package-Independent Computational Chemistry Algorithms, *J. Comput. Chem.* 29 (2008) 839–845.
- [71] Z. Demircioğlu, Ç. Albayrak Kaştaş, O. Büyükgüngör, X-ray structural, spectroscopic and computational approach (NBO, MEP, NLO, NPA, Fukui function analyses) of (E)-2-((4-bromophenylimino)methyl)-3-methoxyphenol, *Mol. Cryst. Liq. Cryst.* 656 (2017) 169–184.
- [72] Y. Megrouss, F. Triki-Baara, N. Boukabcha, A. Chouaih, A. Hatzidimitriou, A. Djafri, F. Hamzaoui, Synthesis, X-ray structure determination and related physical properties of thiazolidinone derivative by DFT quantum chemical method, *Acta Chim. Slov.* 66 (2019) 490–500.
- [73] B. Kosar, C. Albayrak, Spectroscopic investigations and quantum chemical computational study of (E)-4-methoxy-2-[(p-tolylimino)methyl]phenol, *Spectrochimica Acta Part A* 78 (2011) 160–167.

- [74] R. G. Pearson, Chemical hardness and density functional theory, *J. Chem. Sci.* 117 (2005) 369–377.
- [75] G. Saleh, C. Gatti, L. Lo Presti, Non-covalent interaction via the reduced density gradient: Independent atom model vs experimental multipolar electron densities, *Comput. Theor. Chem.* 998 (2012) 148–163.
- [76] E. R. Johnson, S. Keinan, P. Mori-Sanchez, J. Contreras-Garcia, A. J. Cohen, W. Yang, Revealing noncovalent interactions, *J. Am. Chem. Soc.* 132 (2010) 6498–6506.
- [77] E. Scrocco, J. Tomasi, Electronic molecular structure, reactivity and intermolecular forces: An heuristic interpretation by means of electrostatic molecular potentials, *Adv. Quant. Chem.* 103 (1978) 115–193.
- [78] M. Kour, S. Kumar, A. Feddag, S. Andotra, A. Chouaih, V.K. Gupta, R. Kant, S.K. Pandey, Synthesis, characterization, single crystal X-ray and DFT analysis of disubstituted phosphorodithioates, *J. Mol. Struct.* 1157 (2018) 708–715.
- [79] M. Drissi, N. Benhalima, Y. Megrouss, R. Rahmani, A. Chouaih, F. Hamzaoui, Theoretical and experimental electrostatic potential around the m-nitrophenol molecule, *Molecules* 20 (2015) 4042–4054.
- [80] N. Boukabcha, A. Feddag, R. Rahmani, A. Chouaih, F. Hamzaoui, Molecular structure, multipolar charge density study and nonlinear optical properties of 4-methyl-N-[(5-nitrothiophen-2-yl)methylidene] aniline, *J. Optoelectron. Adv. Mater.* 20 (2018) 140–148.
- [81] R. Rahmani, A. Djafri, A. Chouaih, A. Djafri, F. Hamzaoui, A. M. Krallafa, Molecular structure, FT-IR, NMR ($^{13}\text{C}/^1\text{H}$), UV–Vis spectroscopy and DFT calculations on (2Z, 5Z)-3-N(4-methoxy phenyl)-2-N'(4-methoxy phenyl imino)-5-((E)-3-(2-nitrophenyl)allylidene) thiazolidin-4-one, *S. Afr. J. Chem.-S-Afr. T.* 72 (2019) 176–188.
- [82] A. E. Reed, L. A. Curtiss, F. Weinhold, Intermolecular interactions from a natural bond orbital, donor-acceptor viewpoint, *Chem. Rev.* 88 (1988) 899–926.
- [83] F. Weinhold, C. R. Landis, *Chem. Ed: Res & Pract* 2 (CERP; special ‘‘structural concepts’’ issue) (2001) 91–104.
- [84] M. Kaur, Y. S. Mary, H. T. Varghese, C. Y. Panicker, H. S. Yathirajan, M. S. Siddegowda, C. V. Alsenoy, Vibrational spectroscopic, molecular structure, first hyperpolarizability and NBO studies of 40-methylbiphenyl-2-carbonitrile, *Spectrochim. Acta A* 98 (2012) 91–99.
- [85] T. K. Kuruvilla, J. C. Prasana, S. Muthu, J. George, S. A. Mathew, Quantum mechanical and spectroscopic (FT-IR, FT-Raman) study, NBO analysis, HOMO-LUMO, first order hyperpolarizability and molecular docking study of methyl[(3R)-3-(2-methylphenoxy)-3-phenylpropyl]amine by density functional method. *Spectrochim Acta A* 188 (2018) 382–393.
- [86] P. Politzer, J. Murray, The fundamental nature and role of the electrostatic potential in atoms and molecules, *Theor. Chem. Acc.* 108 (2002) 134–142.
- [87] C. Adant, M. Dupuis, J. L. Bredas, Ab initio study of the nonlinear optical properties of urea: Electron correlation and dispersion effects, *Int. J. Quantum Chem.* 56 (1995) 497–507.
- [88] S. Uzun, Z. Esen, E. Koç, N. C. Usta, M. Ceylan, Experimental and density functional theory (MEP, FMO, NLO, Fukui functions) and antibacterial activity studies on 2-amino-4-(4-nitrophenyl) -5,6-dihydrobenzo [h] quinoline-3-carbonitrile, *J. Mol. Struct.* 1178 (2019) 450–457.
- [89] N. Benhalima, N. Boukabcha, Ö. Tamer, A. Chouaih, D. Avci, Y. Atalay, F. Hamzaoui, Solvent effects on molecular structure, vibrational frequencies; and NLO properties of N-(2,3-Dichlorophenyl)-2-Nitrobenzenesulfonamide: a density functional theory study, *Braz. J. Phys.* 46 (2016) 371–383.

- [90] S. Miertus, E. Scrocco, J. Tomassi, Electrostatic interaction of a solute with a continuum. A direct utilization of Ab initio molecular potentials for the prevision of solvent effects, *J. Chem. Phys.* 55 (1981) 117–129
- [91] C. Cassidy, J. M. Halbout, W. Donaldson, C. L. Tang, Nonlinear optical properties of urea, *Opt. Commun.* 29 (1979) 243–246.
- [92] A. Chouaih, F. Hamzaoui, G. Vergoten, Capability of X-ray diffraction to the determination of the macroscopic linear susceptibility in a crystalline environment: the case of 3-Methyl 4-Nitropyridine N-oxide (POM), *J. Mol. Struct.* 738(1-3) (2005) 33–38.
- [93] S. Saravanan, V. Balachandran, Conformational stability, spectroscopic (FT-IR, FT-Raman and UV-Vis) analysis, NLO, NBO, FMO and Fukui function analysis of 4-Hexylacetophenone by density functional theory, *Spectrochim. Acta A Mol. Biomol. Spectrosc.* 138, 2015, 406–423.
- [94] K. Sarojini, H. Krishnan, C. C. Kanakam, S. Muthu, Synthesis, structural, spectroscopic studies, NBO analysis, NLO and HOMO-LUMO of 4-methyl-N-(3-nitrophenyl)benzene sulfonamide with experimental and theoretical approaches, *Spectrochim. Acta A Mol. Biomol. Spectrosc.* 108 (2013) 159–170.
- [95] T. Hamada, An ab Initio Molecular Orbital Study on Hyperpolarizabilities of an Interacting 2-Methyl-4-nitroaniline Molecular Pair: A Molecular Study on the Oriented-Gas Approximation, *J. Phys. Chem.* 100(21) (1996) 8777–8781.
- [96] T. Kodaira, A. Watanabe, O. Ito, M. Matsuda, K. Clays, A. Persoons, Evaluation of hyperpolarizability of nonlinear optical organic molecules by hyper-Rayleigh scattering, *Jpn. J. Appl. Phys.* 35 (1996) 6074–6078.
- [97] T. Gnanasambandan, S. Gunasekaran, S. Seshadri, Experimental and theoretical study of p-nitroacetanilide, *Spectrochim. Acta A Mol. Biomol. Spectrosc.* 117 (2014) 557–567.
- [98] O. Y. Borbulevych, R. D. Clark, A. Romero, L. Tan, M. Y. Antipin, V. N. Nesterov, B. H. Cardelino, C. E. Moore, M. Sanghadasa, T. V. Timofeeva, Experimental and theoretical study of the structure of N,N-dimethyl-4-nitroaniline derivatives as model compounds for non-linear optical organic materials, *J. Mol. Struct.* 604(1) (2002) 73–86.
- [99] M. Lequan, C. Branger, J. Simon, T. Thami, E. Chauchard, A. Persoons, Hyperpolarizability of tetraorganotin compounds determined by the hyper-Rayleigh scattering technique, *Chem. Phys. Lett.* 229 (1994) 101–104.
- [100] J.L. Oudar, R. Hierle, An efficient organic crystal for nonlinear optics: methyl-(2,4-dinitrophenyl)-aminopropanoate, *J. Appl. Phys.* 48 (1977) 2699–2704.

Scheme and Figures



Reagents and conditions: (a) $\text{BrCH}_2\text{COOC}_2\text{H}_5$, acetone, reflux; (b) $\text{NH}_2\text{NH}_2 \cdot \text{H}_2\text{O}$, ethanol, reflux; (c) para-nitrobenzaldehyde, ethanol, reflux.

Scheme 1 Chemical pathways of NBQA formation.

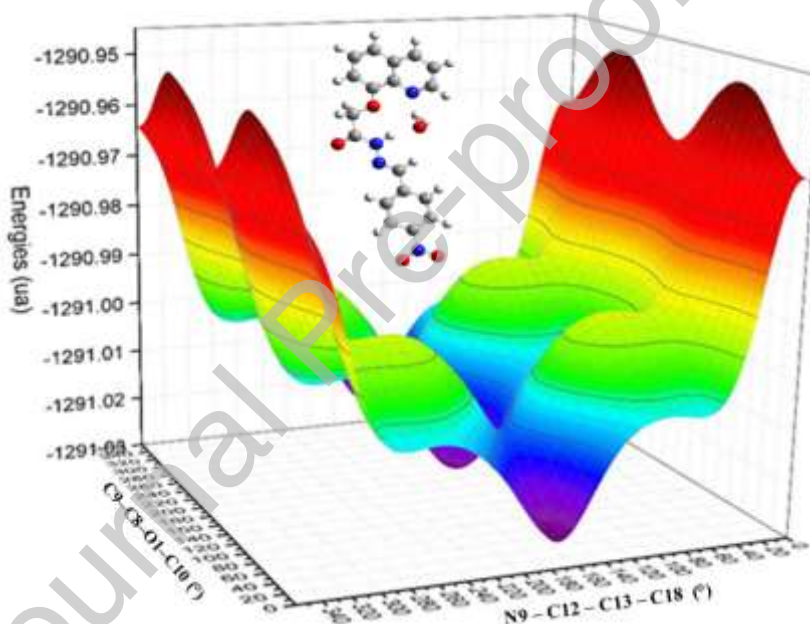
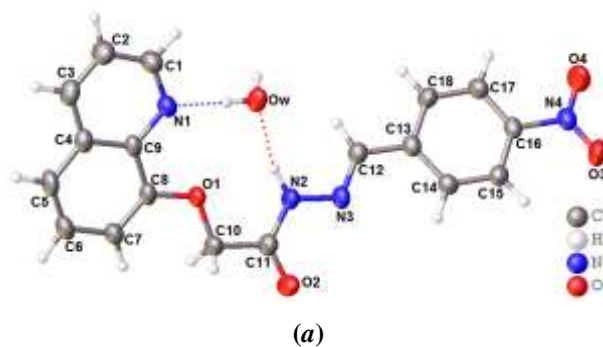


Fig. 1 3D plot of potential energy surfaces of the title molecule obtained by using BPV86/6-311G(d,p)



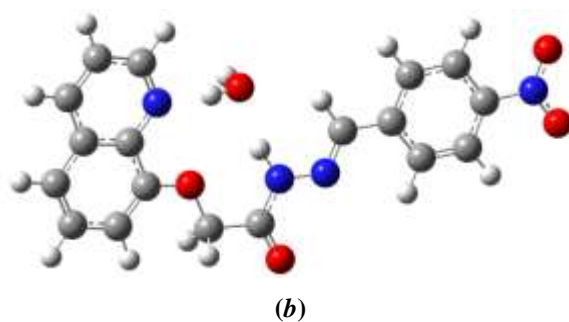


Fig. 2 General view of the molecular geometry for NBQA: (a) the X-ray structure and (b) the optimized structure at BPV86/6-311G(d,p)

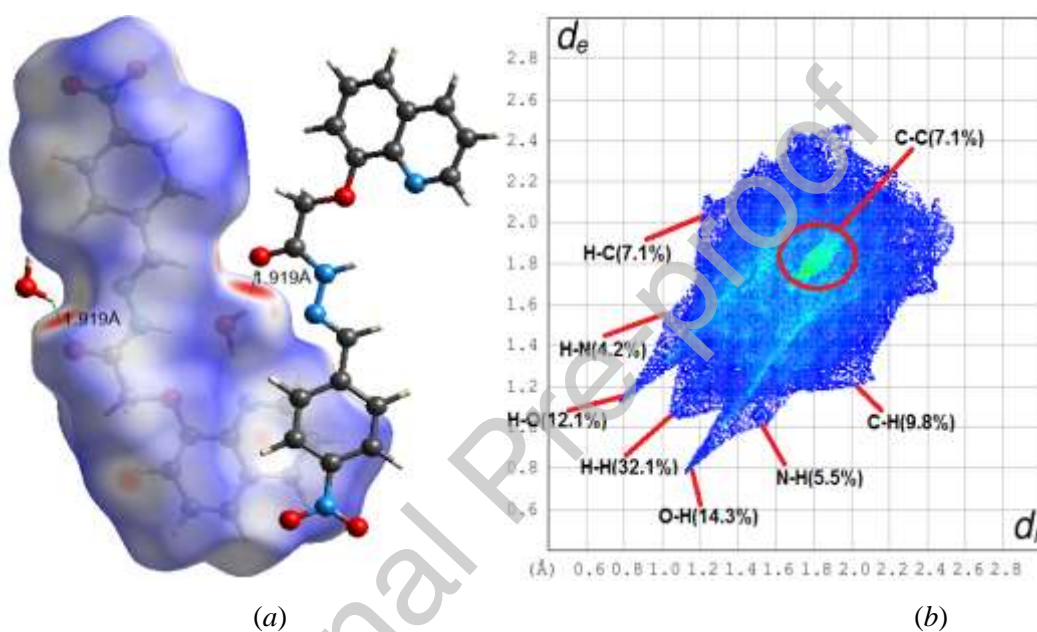
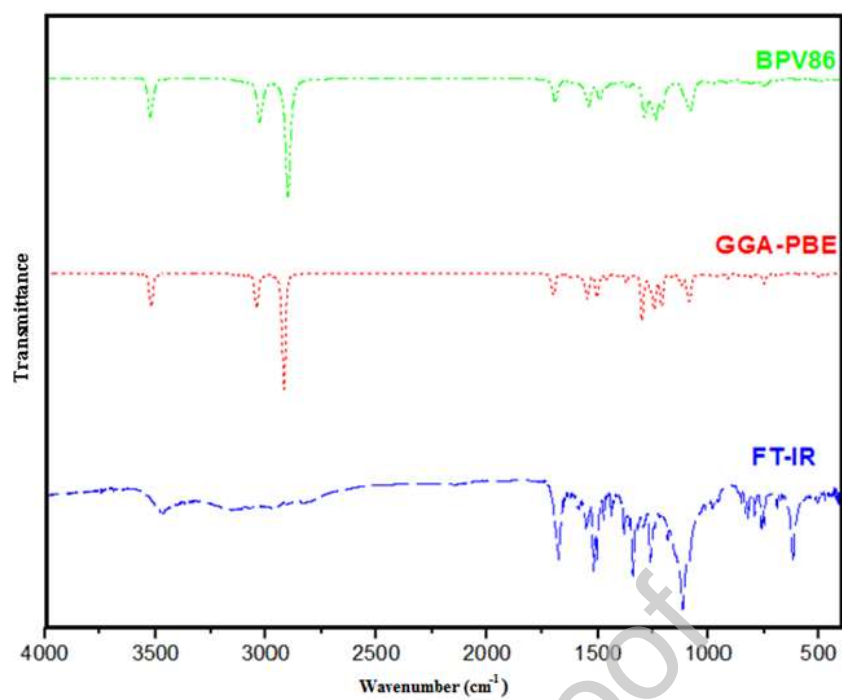
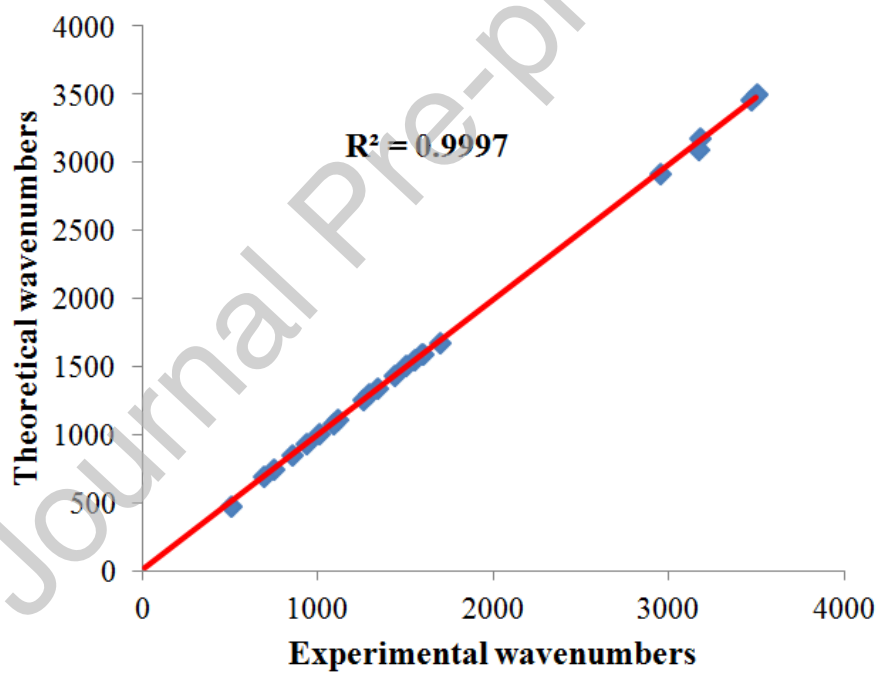


Fig. 3 HS view of NBQA (a) 3D HS mapped over dnorm and (b) 2D fingerprint plot.



(a)



(b)

Fig. 4 (a) FT-IR spectrum and simulated (BPV86, PBE) IR spectra for NBQA, (b) Experimental and DFT/BPV86-IR correlation of NBQA

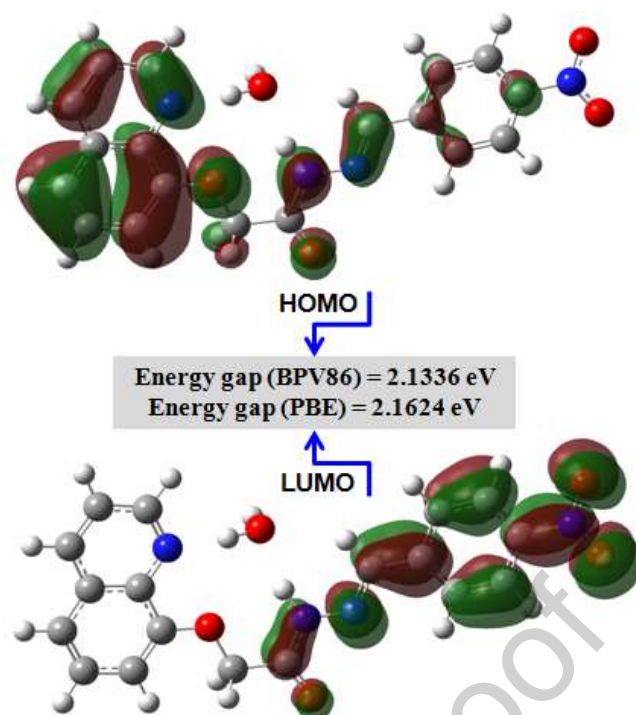
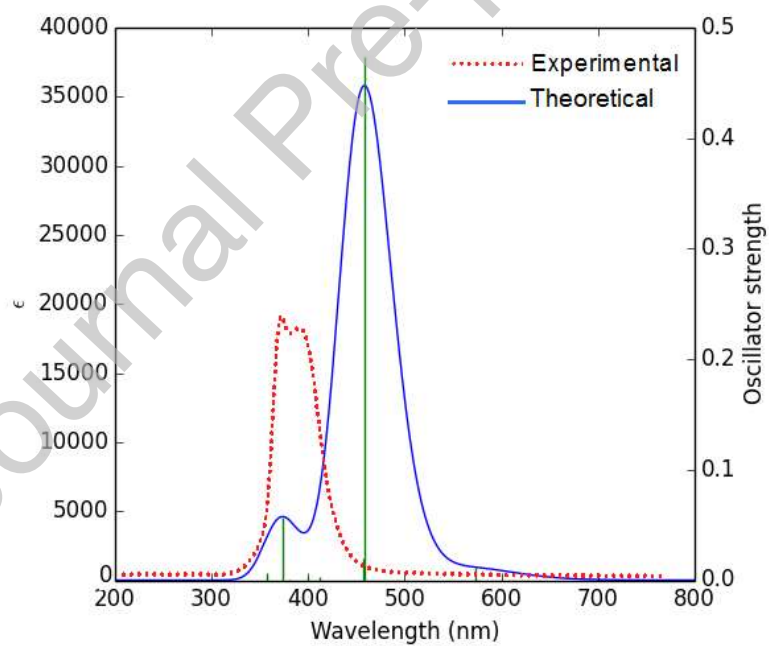


Fig. 5 HOMO-LUMO plot for NBQA with BPV86/6-311G(d,p) approach.



(a)

Fig. 7 2D scatter and Isosurface density plots illustrating the non-bonded interactions of NBQA

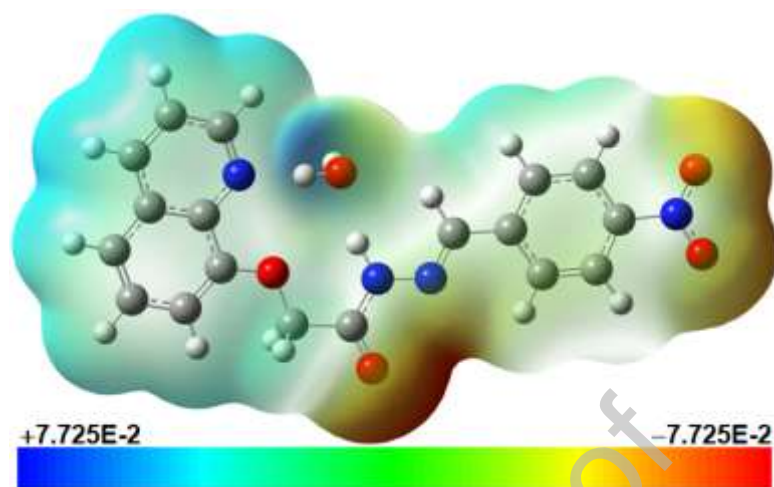


Fig. 8 MEP picture for the title compound at BPV86/6–311G (d,p) level

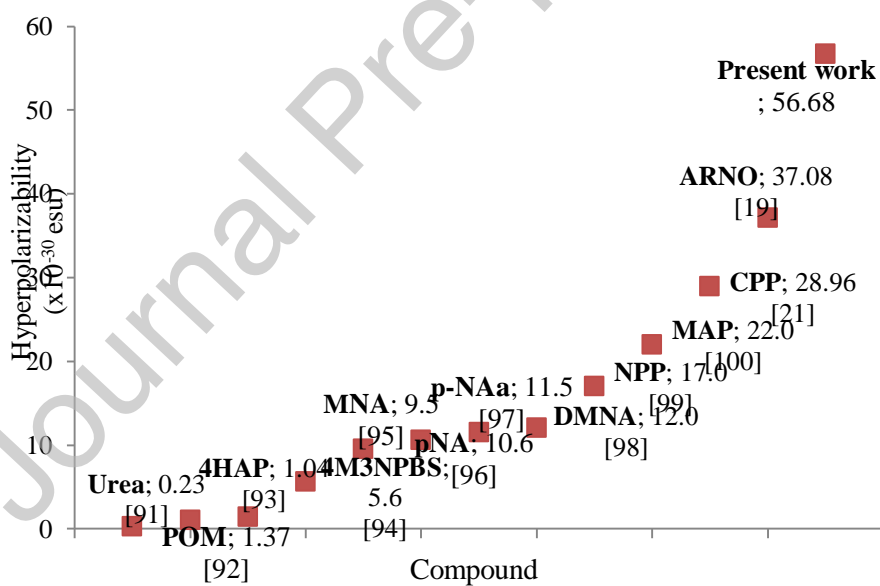


Fig. 9 Comparison between hyperpolarizabilities (β) of some NLO compounds

Table 1 Experimental conditions and crystallographic details

Empirical formula	C ₁₈ H ₁₄ N ₄ O ₄ , H ₂ O
CCDC reference no.	2006263
Formula weight	368.35
Crystal size (mm)	0.20 × 0.18 × 0.16
Temperature (K)	173(2)
Crystal system, space group	Monoclinic, C2/c
Unit cell dimensions	
a (Å)	21.885(2)
b (Å)	11.896(2)
c (Å)	13.042(2)
β (°)	92.620(10)
Wavelength (Å)	0.71073
Volume (Å ³)	3391.9(8)
Z, calculated density (Mg/m ³)	8/1.443
F(000)	1536
θ range for data collection	3.28 – 28.07
Limiting indices	−27 ≤ h ≤ 26, −15 ≤ k ≤ 14, −16 ≤ l ≤ 17
Reflections collected/unique observed with I ≥ 2σ(I)	3567/2700
Refinement method	Full-matrix least-squares on F ² data
Parameters	309
Goodness of fit on F ²	1.014
Final R indices	
R ₁	0.0368
wR ₂	0.0858
R indices (all data)	
R ₁	0.0544
wR ₂	0.0948

Table 2 Hydrogen-bonds (Å, °)

D—H...A	D—H	H...A	D...A	D—H...A
C12—H12...Ow	0.954 (16)	2.541(16)	3.249 (18)	131.1 (12)
N2—H...O1	0.909 (18)	2.315(16)	2.664 (14)	102.6 (12)
N2—H...Ow	0.909 (18)	1.905(18)	2.793 (18)	165.2 (15)
Ow—HwA...O1	0.91 (2)	2.588(18)	3.021 (15)	110.1 (13)
Ow—HwA...N1	0.91 (2)	1.88 (2)	2.783 (16)	172.5 (17)
Ow—HwB...O2 ⁽ⁱ⁾	0.87 (2)	2.01(2)	2.743 (16)	142 (2)
C12—H12...O2 ⁽ⁱⁱ⁾	0.954 (16)	2.455 (17)	3.377 (2)	162.3 (13)
C7—H7...Ow ⁽ⁱⁱⁱ⁾	0.958 (16)	2.434 (16)	3.211 (2)	137.9 (12)
C1—H1...O4 ⁽ⁱⁱⁱ⁾	0.964 (17)	2.455 (16)	3.097 (2)	123.9 (12)

Symmetry codes : (i) $-x+1/2, y-1/2, -z+1/2$; (ii) $x, -y+1, z-1/2$; (iii) $-x+1/2, -y+1/2, -z+1$.

Table 3 Calculated energy values and thermodynamic parameters for NBQA at BPV86 and PBE functionals with 6-311G(d,p)

Parameters	BPV86	GGA-PBE
E _{HOMO} (eV)	−5.7676	−5.6574
E _{LUMO} (eV)	−3.6340	−3.4940
E _{HOMO} − E _{LUMO} gap (eV)	2.1336	2.1624
Ionization potential I (eV)	5.7676	5.6574
Electron affinity A (eV)	3.6340	3.4940
Electronegativity χ	4.7008	4.5762
Chemical potential P	−4.7008	−4.5762
Chemical hardness η	1.0668	1.0812
Chemical softness S (eV)	0.4687	0.4625
Electrophilicity index ω	10.3569	9.6841

Zero-point vibrational energy (Kcal.mol ⁻¹)	197.4181	197.8642
Zero-point correction (Hartree/Particle)	0.3146	0.3153
Thermal correction to energy	0.3389	0.3396
Thermal correction to enthalpy	0.3399	0.3406
Thermal correction to Gibbs free energy	0.2573	0.2582

Table 4 Experimental wavelength and calculated electronic transitions for NBQA using TD-DFT/BPV86 method with the 6-311G(d,p) basis set in chloroform solvent

Experimental λ (nm)	Theoretical			
	λ (nm)	Osc. strength (<i>f</i>)	Energy (eV)	Major contributions ($\geq 10\%$)
384	572.79	0.0116	2.1646	HOMO→LUMO (43%)
	458.47	0.4740	2.7043	HOMO-1→LUMO (78%) HOMO→LUMO (12%)
	456.65	0.0197	2.7151	HOMO-2→LUMO (96%)
	411.71	0.0027	3.0114	HOMO-1→LUMO+1 (64%) HOMO→LUMO+1 (36%)
	399.72	0.0026	3.1018	HOMO-3→LUMO (99%)
	381.16	0.0001	3.2528	HOMO-6→LUMO (20%) HOMO-5→LUMO (79%)
	380.08	0.0001	3.2620	HOMO-6→LUMO (79%) HOMO-5→LUMO (19%)
	372	373.95	0.0573	3.3155
370.70		0.0001	3.3446	HOMO-4→LUMO (98%)
357.81		0.0069	3.4651	HOMO-1→LUMO+2 (15%) HOMO→LUMO+2 (84%)

Table 5 Second order perturbation theory analysis of Fock matrix in NBO basis for NBQA

Donor (i)	Type of bond	ED (i)(e)	Acceptor (j)	Type of bond	ED (j)(e)	E ⁽²⁾ (kcal/mol)	($\epsilon_j - \epsilon_i$) (a.u)	F(i, j) (a.u)
C1-N1	π	1.80479	C2-C3	π^*	0.22730	10.40	0.35	0.054
C1-N1	π	1.80479	C4-C9	π^*	0.45709	18.59	0.34	0.076
C2-C3	π	1.70538	C1-N1	π^*	0.32863	26.69	0.27	0.076
C2-C3	π	1.70538	C4-C9	π^*	0.45709	15.47	0.29	0.062
C4-C9	π	1.54485	C1-N1	π^*	0.32863	15.93	0.25	0.058
C4-C9	π	1.54485	C2-C3	π^*	0.22730	17.26	0.28	0.066
C4-C9	π	1.54485	C5-C6	π^*	0.25298	14.30	0.29	0.061
C4-C9	π	1.54485	C7-C8	π^*	0.31989	17.01	0.28	0.064
C5-C6	π	1.74717	C4-C9	π^*	0.45709	18.19	0.28	0.067
C5-C6	π	1.74717	C7-C8	π^*	0.31989	15.82	0.28	0.061
C7-C8	π	1.72614	C4-C9	π^*	0.45709	14.84	0.29	0.061
C7-C8	π	1.72614	C5-C6	π^*	0.25298	18.35	0.31	0.068
C12-N3	π	1.90989	C13-C18	π^*	0.36341	10.01	0.35	0.057
C13-C18	π	1.59838	C12-N3	π^*	0.18047	16.96	0.27	0.064
C13-C18	π	1.59838	C14-C15	π^*	0.25911	16.77	0.28	0.064
C13-C18	π	1.59838	C16-C17	π^*	0.38919	24.39	0.27	0.073
C14-C15	π	1.66311	C13-C18	π^*	0.36341	20.58	0.28	0.069
C14-C15	π	1.66311	C16-C17	π^*	0.38919	19.55	0.27	0.066
C16-C17	π	1.64084	C13-C18	π^*	0.36341	17.38	0.29	0.064
C16-C17	π	1.64084	C14-C15	π^*	0.25911	19.09	0.30	0.069
C16-C17	π	1.64084	N4-O3	π^*	0.63834	32.11	0.14	0.064
N4-O3	π	1.98611	O4	n_3	1.46093	11.81	0.17	0.077
C1-N1	π^*	0.32863	C2-C3	π^*	0.22730	83.92	0.03	0.082
C1-N1	π^*	0.32863	C4-C9	π^*	0.45709	133.87	0.02	0.074
C4-C9	π^*	0.45709	C5-C6	π^*	0.25298	141.13	0.02	0.077

C7-C8	π^*	0.31989	C5-C6	π^*	0.25298	168.97	0.01	0.077
C12-N3	π^*	0.18047	C13-C18	π^*	0.36341	146.44	0.01	0.067
C16-C17	π^*	0.38919	C14-C15	π^*	0.25911	171.53	0.02	0.080
N4-O3	π^*	0.63834	C16-C17	π^*	0.38919	16.07	0.15	0.061
O1	n_2	1.84059	C7-C8	π^*	0.31989	30.83	0.35	0.096
O2	n_2	1.86135	C10-C11	σ^*	0.06337	20.44	0.62	0.102
O2	n_2	1.86135	C11-N2	σ^*	0.08175	26.93	0.71	0.125
O3	n_2	1.90260	C16-N4	σ^*	0.09809	11.81	0.59	0.074
O3	n_2	1.90260	N4-O4	σ^*	0.05664	19.16	0.70	0.105
O4	n_2	1.90254	C16-N4	σ^*	0.09809	11.82	0.59	0.074
O4	n_2	1.90254	N4-O3	σ^*	0.05655	19.14	0.70	0.105
O4	n_3	1.46093	N4-O3	π^*	0.63834	158.99	0.14	0.138
N2	n_1	1.61217	C11-O2	π^*	0.29650	63.80	0.27	0.120
N2	n_1	1.61217	C12-N3	π^*	0.18047	28.46	0.27	0.083
N3	n_1	1.93757	C12-H12	σ^*	0.03232	10.00	0.85	0.081

Table 6 Atomic charges distribution for NBQA calculated by Mulliken and the natural bond orbital (NBO) methods using the BPV86/6–311G(d,p) level in gas phase.

Atoms	NBO	Mulliken	Atoms	NBO	Mulliken
O1	-0.513	-0.338	C14	-0.175	-0.047
O2	-0.597	-0.357	C15	-0.189	-0.072
O3	-0.386	-0.270	C16	0.061	0.159
O4	-0.387	-0.271	C17	-0.189	-0.069
Ow	-0.959	-0.533	C18	-0.183	-0.086
N1	-0.500	-0.467	H1	0.203	0.137
N2	-0.410	-0.299	H2	0.230	0.135
N3	-0.244	-0.193	H3	0.226	0.128
N4	0.478	0.119	H5	0.223	0.117
C1	0.077	0.109	H6	0.223	0.129
C2	-0.241	-0.212	H7	0.233	0.149
C3	-0.135	0.071	H10a	0.215	0.172
C4	-0.079	-0.153	H10b	0.214	0.173
C5	-0.214	-0.071	H12	0.202	0.120
C6	-0.178	-0.112	H14	0.238	0.126
C7	-0.292	-0.132	H15	0.247	0.149
C8	0.328	0.192	H17	0.247	0.147
C9	0.149	0.180	H18	0.227	0.129
C10	-0.144	-0.098	H	0.422	0.291
C11	0.642	0.307	Hw1	0.465	0.265
C12	0.033	0.114	Hw2	0.492	0.313
C13	-0.061	-0.152			

Table 7 Dipole moments (Debye), molecular polarizabilities ($\times 10^{-24}$ esu) and hyperpolarizabilities ($\times 10^{-30}$ esu) in different solvents of the title compound.

Solvent	μ		α		β		$E_{\text{HOMO}}-E_{\text{LUMO}}$ (ev)	
	BPV86	PBE	BPV86	PBE	BPV86	PBE	BPV86	PBE
Gas ($\epsilon = 1$)	13.67	13.54	44.97	44.85	56.68	55.98	2.35	2.37
CCl_4 ($\epsilon = 2.2$)	15.18	15.02	52.91	52.73	109.23	106.26	2.24	2.26
Diethylether ($\epsilon = 4.3$)	15.89	15.71	56.96	56.74	143.72	139.20	2.15	2.18
Chloroform ($\epsilon = 4.9$)	15.96	16.01	57.46	57.23	148.46	143.77	2.13	2.16
Acetone ($\epsilon = 20.7$)	16.57	16.39	61.20	60.93	188.06	181.84	2.00	2.04
Ethanol ($\epsilon = 24.5$)	16.61	16.42	61.41	61.14	190.51	184.20	1.99	2.03
Acetonitrile ($\epsilon = 36.6$)	16.65	16.47	61.72	61.44	194.10	187.64	1.98	2.02
DMSO ($\epsilon = 46.7$)	16.68	16.49	61.89	61.61	196.09	189.55	1.98	2.01
Water ($\epsilon = 78.4$)	16.71	16.53	62.10	61.83	198.71	192.06	1.97	2.00